WALL INTERFERENCE EFFECTS ON STEADY FORCE CO-EFFICIENTS OF BLUFF BODIES

Cheong-Pak Ng

A RESEARCH THESIS

in the

Faculty of Engineering

Presented in partial fulfillment of the requirements for
the Degree of MASTER OF ENGINEERING
at
Sir George Williams University
Montreal, Canada

July 1972

A B S T R A C T

It is well documented that side walls interference effects can alter the steady hydrodynamic force coefficients of single bluff bodies set in a narrow channel. The variation of the steady drag and lift coefficients for a two dimensional circular cylinder and a triangular prism due to wall interference are reported here for a large range of blockage ratios. The effect of wall constraint on the Strouhal frequency is also examined for a limited range of blockage ratios. The gap velocity and the contracted jet velocity are used to normalise the steady force coefficients and the vortex shedding frequency. The resulting dimensionless parameters are shown to be generally constant in the range of blockages tested.

A C K N O W L E D G E M E N T

The Author wishes to thank Dr. A.S. Ramamurthy for suggesting the thesis topic. The assistance of Messrs. Ted. Mani, Tom Dugdale and Herman Termors is highly appreciated. Part of the electronics equipment used in the project was procured through N.R.C. Grant No. A7608.

TABLE OF CONTENTS

LIST OF TABLES..... iv

LIST OF FIGURES..... v

LIST OF SYMBOLS..... vi

INTRODUCTION..... 1

ANALYTICAL METHODS..... 1

EXPERIMENTAL METHODS..... 5

EXPERIMENTAL SET UP AND PROCEDURES..... 10

ANALYSIS OF RESULTS..... 11

Steady Force Coefficients..... 12
Vortex Shedding Frequency..... 14

SUMMARY AND CONCLUSIONS..... 16

SCOPE FOR FURTHER STUDIES..... 17

APPENDIX 1 - Some Definitions..... 18

APPENDIX 2 - Bibliography..... 21

APPENDIX 3 - Figures..... 24

APPENDIX 4 - Existing Strouhal Number Propositions..... 50

APPENDIX 5 - Data Comparison..... 54

APPENDIX 6 - Calibration Data (Velocity Distribution, Transducer Calibration, Force Gage Computation)..... 61

APPENDIX 7 - Computer Programs and Outputs..... 63

LIST OF TABLES

Tables		Pages
1.	Drag coefficients C_D, C_{D1} - Cylinder.	55
2.	Drag coefficients C_D, C_{D1} and C_{Dj} - Plate and triangle prism.	56
3.	Drag & lift coefficients C_D, C_{D1}, C_L and C_{L1} - Triangle prism.	57
4.	Strouhal number S and S_1 - Cylinder.	58
5.	Strouhan number S and S_1 - Triangle prism.	59
6.	Strouhal number S, S_1 and S_j - Plate,gate and triangle prism.	60
7.	Steady Force coefficients program.	64
8.	Drag & Lift coefficients-Reduced data, 1" Body,b/B=0.071	65
9.	Drag & Lift coefficients-Reduced data, 2" Body,b/B=0.141	66
10.	Drag & Lift Coefficients-Reduced data, 3" Body,b/B=0.212	67
11.	Drag & Lift coefficients-Reduced data, 4" Body,b/B=0.282	68
12.	Drag & Lift coefficients-Reduced data, 6" Body,b/B=0.423	69
13.	Drag & Lift coefficients-Reduced data, 8" Body,b/B=0.564	70
14.	Drag & Lift coefficients-Reduced data,10" Body,b/B=0.705	71
15.	Strouhal Number Program	72
16.	Strouhal Number-Reduced data, 1" Body, b/B=0.071	73
17.	Strouhal Number-Reduced data, 2" Body, b/B-0.141	74
18.	Strouhal Number-Reduced data, 3" Body, b/B=0.212	75
19.	Strouhal Number-Reduced data, 4" Body, b/B=0.282	76
20.	Strouhal Number-Reduced data, 6" Body, b/B=0.423	77
21.	Vortex Street characteristics program.	78
22.	Output-Vortex street program.	79

LIST OF FIGURES

Figure:		Page
1.	Constricted Flow	24
2.	Parameter Range	25
3.	Test Section	26
4.	Instrumentation	27
5.	C_D Vs Reynolds No., Prism θ=60°	28
6.	C_D Vs Reynolds No., Prism θ=30°	29
7.	C_D Vs Reynolds No., Prism θ=0°	30
8.	C_D & C_{D1} Vs Blockage, Prism θ=60°	31
9.	C_D & C_{D1} Vs Blockage, Prism θ= 30°	32
10.	C_D, C_{D1} & C_{Dj} Vs Blockage, Prism θ=0°	33
11.	Effect of θ on C_D & C_L.	34
12.	C_L Vs Reynolds No., Prism θ=30°	35
13.	C_L & C_{L1} Vs Blockage, Prism θ=30°	36
14.	C_D & C_{D1} Vs Reynolds No., Cylinder	37
15.	S Vs Reynolds No., Prism	38
16.	S Vs Reynolds No., Cylinder	39
17.	S Vs Blockage, Prism	40
18.	S & S_1 Vs Blockage, Cylinder	41
19.	S_1 & S_j Vs Blockage, Prism	42
20.	Velocity Distribution at the test section	43
21.	Transducer Calibration; Volt Vs lb.	44
22.	Stiffness of the Force Gauge	45
23.	Strip Chart Recorder	46
24.	Spectral Plots	47
25.	Photograph of Equipment	48
26.	Eccentric Mounting Partial Row Equivalence	49

LIST OF SYMBOLS

Symbol	Description
b	Side of the equilateral triangular prism (for all $\theta=0°$, $30°$ and $60°$, Fig.2)
b_1	Gap width (Fig.1)
b'	Maximum wake width in 2-d flows (=maximum wake area in axisymmetric flows)
B	Test section width. (=Test section area in axisymmetric flows)
$\frac{b}{B}$	Blockage (Wall constraint)
c	Chord length
C_c	Contraction coefficient
C_D	Drag coefficient normalised by u
C_{D1}	Drag coefficient normalised by u_1
C_{Dj}	Drag coefficient normalised by u_j
C_L	Lift coefficient normalised by u
C_{L1}	Lift coefficient normalised by u_1
C_p^*	Pressure coefficient behind the plate
d	Diameter of the circular cylinder (Fig.2)
f	Frequency of vortex shedding
k	An emphirical constant
L	Span of the body ($\simeq$10" in the present tests)
K	Stiffness (lb/in) of gauge.
P	Load (lb)

List of Symbols (contd.)

Symbol	Description
P_b	Base pressure
P_w	Wake pressure
R	Reynolds number
R_c	Critical Reynolds number
S	Strouhal number normalised by u
S_1	Strouhal number normalised by u_1
S_j	Strouhal number normalised by u_j
S*	Universal Strouhal number
u	The mean undisturbed velocity at the center line of model location.
u_1	Mean gap velocity (Fig.1)
u_j	Mean velocity of the jet at the vena contracta (contracted jet velocity $\simeq u_s$ for higher blockages)
u_s	Velocity at the separation point (=ku, see Fig.1)
ρ	Density of fluid (air)
ν	Kinematic viscosity of fluid (air)
θ	Orientation of the body (plate, prism, etc.)
β	Damping coefficient of gauge.
β_c	Critical damping coefficient of gauge.
ζ	Damping ratio.
δ	Deflection of gauge (in).

INTRODUCTION

The need to use a model relatively large, compared to the test section dimensions in model simulation occurs due to the imposed physical limitations. Some of these may be related to the sensitivity of instrumentation, which requires a threshold value of a physical variable to be present for effective recording (higher signal to noise ratio). In some applications, one may be forced to provide a large obstruction in a relatively small area as in air ducts. In such cases, power estimates which depend on the pressure losses can be easily obtained once the force coefficient data is available for these oversized obstacles. When the model is larger, the construction of a geometrically similar body is simpler, as considerable detail can be incorporated in it with ease. From a purely practical view point, much of model testing is done in flows bound by side walls while the prototype applications are generally in unlimited flows. All these factors indicate thatwall interference data is needed in practical applications.

The results of blockage study on single bodies will often provide some qualitative leads related to interference effects caused by adjacent members in grouped bodies. Interference of flow past groups of bodies include applications in heat exchanger tubes[1,2,3], ocean piles[4], bridge piers[5] and grouped buildings.

ANALYTICAL METHODS

Glauret[6] discussed the characteristics of interference effects and classified them for purposes of mathematical modelling.

Maskell[7] provided a correction formula based on the concept of a quasi steady wake bubble. He used momentum balance arguments and estimated the effective increase in the velocity due to wall interference. He checked his theory based on the data

of Fail[8]. He explained constraint (blockage - see appendix 1) as an excess in the dynamic pressure. This implies a dynamic similarity which renders the pressure distribution to be invariant when the body is set in a narrow channel except for a scaling factor which depends on the base pressure P_b. In other words, C_D/k^2 is to be constant,

where,

C_D = the drag coefficient, and

u_s = ku denotes the separation velocity

u = the undisturbed velocity

k = an emphirical constant.

Shaw's results[9] for flat plates indicate that the contribution of the down stream section is the predominant factor in determining the magnitude of the drag at higher blockages. Since the value of k is closely related to the base pressure coefficient, Shaw's results lend support to the invariance of C_D/k^2 for large blockages. While striking a momentum balance between the down stream section at the vena contracta and the section far upstream of the body, Maskell assumes that the factor $(b'/B)^2$ is small (Fig.1). Here, (b'/B) is the ratio of wake area b' (Fig.1) to test section area B. As such, Maskell's theory is only of very limited use. Further, one also notes that the data used by Maskell to support his theory are related to tests where the blockage was limited to 0.045. For flow past bluff objects, increased blockage results in increased values of u_s, the velocity at the point of separation. This results in forebody pressure distributions[9] that are no longer normalised by a simple increment in the velocity. This invalidates Maskell's assumption related to dynamic similarity, although the gross characteristics such as the steady drag force for blocked flows can still be handled by giving an increment to u, the undisturbed velocity.

Modi[10] presented an interesting discussion about blockage theories and asserts that Maskell's theory fails to corelate his data for larger blockages. He suggested that higher order terms be used in Maskell's expression to obtain a modest improvement in correlating his own data. Any theory which tries to accommodate the constriction effects by providing a simple increment to the velocity (or indirectly the dynamic pressure) fails to properly account for interference characteristics where boundary layer effects control the wake dynamics of bluff bodies, such as circular cylinders. This criticism is true of Maskell's theory as well as the present simple proposition advanced in this report. The results presented in a subsequent section for the circular cylinders will bear testimony to this fact.

Toebes[11] questioned Maskell's assumption about the wake pressure P_w being equal to the base pressure P_b. It is admitted that even the near wake is dynamic. However, for want of an alternative procedure, this assumption though weak may not by itself lead to erroneous assesment of steady force parameters. Toebes[12] earlier provided a critical apprisal of the hodograph methods. He provided a new expression to link the steady drag and the oscillatory lift with the help of a dynamic model.

Sarpkaya[13] used complex variable techniques to obtain the characteristics of flow past a two dimensional plate set at different angles in a conduit. Specifically, he obtained expressions for the contraction coefficient C_c of butterfly valves. Observe that the maximum width of the wake in constricted flows is readily obtained when one determines the contraction coefficient C_c (Fig.1). For higher blockages, Shaw[14] observes that "Although the concept of a free streamline bounding the issuing jet does not strictly apply when diffusion of the jet occurs, the velocity of the jet at the separation point (u_s) is still equal to that over the core of the jet (u_j) at the vena contracta". This suggests that B/b,

C_c, k and hence u_s are interrelated (Fig.1). As such, the coefficient of contraction C_c is an important parameter for confined flows.

As a matter of fact, the above assumption of velocity invariance along the free streamline up to the region where the wake reaches its maximum width is taken for granted in the classical free streamline models[15] and their modifications[16]. On the other hand, when we connect u_s with C_c in unconfined flows, we run into difficulty. Unconfined flows can be considered as the limit of constricted flows and this gives the absurd result of the separation velocity u_s being equal to u according to earlier arguments (C_c=1 for unconfined flow). Shaw[9] recognised the above facts in his elegant analysis of the wall constraint problem as applied to a normal flat plate. He adopted complex variable techniques to arrive at the characteristics of the blocked flow. The application of his results to practical cases should be limited (lower limit) to constrictions where u_s equals the velocity u_j at the section where the wake is largest (i.e. at the vena contracta). Shaw provided collaborating evidence to his theoretical predictions using his test data which appear to be very convincing.

Abernathy[17] presented the solution to the constricted flow problem related to flat plates set at an angle of incidence. He uses a modified form of the notched hodograph theory[16] related to unconfined flows and provides collaborating experimental evidence to show that the separation "b'" between the vortex sheets for flow past a flat plate is 1.41 c sinΘ over a wide range of blockage ratios. Here c is the chord length and Θ is the angle of attack. Using the above value of b' as the characteristic length which is said to be independent of the flow constriction, a universal Strouhal number S* is formed similar to Roshko's[16] proposal. According to Abernathy's test data, S* remains invariant for a wide range of plate inclination Θ and blockage. S* itself is defined as:

$$S^* = \frac{f\ 1.41\ c\ \sin\Theta}{\sqrt{1 - C_p^*}\ u}$$

where,

C_p^* = the pressure coefficient behind the plate

f = the frequency of vortex shedding

Θ = the angle of attack

u = the velocity far upstream

EXPERIMENTAL METHODS

Tozkas[18] examined the effect of flow confinement on the two dimensional cylinders and sharp edged plates on the Strouhal number. He observed that the universal Strouhal number S* based on the wake width b' and wake velocity u_s remains invariant only in a limited blockage range. Chen[19] extended this investigation and included a 90° wedge as the test body to check the validity of Roshko's universal Strouhal number[16] concept. The usual definition of the Strouhal number S is related to S* as follows:

$$S = \frac{fd}{u} \qquad ..(2)$$

$$S^* = \frac{fb'}{u_s} = \frac{S\ b'}{k\ d} \qquad ..(2a)$$

u = undistributed velocity

$u_s = k\ u$ = velocity at the separation point ..(3)

b' = wake width, d = width of body, and

f = frequency of vortex shedding.

For the flow past a 90° wedge, Chen used the theoretical contraction coefficients derived by Von Mises [15]. In so doing, one should keep in mind the physical limitation of the lower bounds of C_p^* in hydraulic flows. He concludes that the dominant frequency of vortex shedding becomes weaker when the blockage ratio b/B reaches a value of 0.6. As a matter of fact, when the blockage is very high, the jet flow emerging from either end of the body is unlikely to interact to form the common Karman vortex trail in the wake. Vortex shedding can occur, even in the absence of interaction among shear layers. For instance, behind a partly closed sharp edged gate which constricts the flow[20], vorticies are formed and lead to gate vibration.

Lin[21] has conducted an experimental investigation into the effect of blockage on the drag coefficient of axisymmetric bodies. He concludes that hemispheres set in constricted flows possess drag coefficients C_D which cannot be explained by a simple increase in the velocity. Nevertheless, he does observe that the predominant portion (98%) of the total drag on the hemisphere is caused by the suction associated with the base pressure. This conclusion demonstrates (see Appendix 1) that C_D/k^2 is nearly invariant. It upholds the fact that C_D for blocked flow is obtained when u is replaced by u_s in the steady drag formula. The increased velocity u_s is related to the velocity u as in equation (3). Lin[22] solved the problem of confined flow past two dimensional wedges using complex variable techniques related to triply connected domains and confirmed his findings using smoke tunnel test data related to the length of separated region and the circulation along the free streamline.

Achenback[23] investigated the effect of blockage on spheres set in a tube. His tests covered a wide range of blockages and Reynolds numbers. Cecin[24] determined the drag coefficient of an axisymmetric body, namely the circular cylinder, whose axis was parallel to the direction of motion. He used the falling body method to obtain the drag coefficients of the cylinders

for a range of blockages. Unfortunately, no attempt was made to group the results and interpret them in terms of blockage effects. The drag coefficient data is essentially linear between the blockage ratios of 0.24 to 0.74, although a curve seems to have been fitted to the data by the authors. McKeon[25] obtained C_D for normal circular plates subject to varying degrees of blockage. He remarks that Maskell's correction methods failed to correlate his data.

Toebes[12] has presented experimental data related to the Strouhal frequency and hydrodynamic lift force for circular cylinders and triangular prisms upto a blockage of 0.445. On the basis of the reported data, he demonstrated that the contracted jet velocity u_j and the gap velocity u_1 (Fig.1) were useful velocity scales to formulate the Strouhal number. u_j and u_1 are readily obtained by continuity arguments. As observed earlier, the replacement of u by u_j to form the velocity scale in the definition of the Strouhal number leads to some difficulties in unconfined flows and weakly confined flows. This criticism is valid even here. The use of u_j to normalise the dynamic lift by Toebes was not successful. This is understandable as the contracted jet velocity u_j was tied to a quasi steady model which disregards the dynamics of the near wake flow. If reasonable comparison of such dynamic forces are to be made, the aspect ratio of the models must be identical and the body dimensions should bear a proper scale to the turbulence scales present in the approaching flow. Toebes[11] investigated the near wake flow field of a triangular prism. He points out the discrepancy between the actual wake bubble geometry and the generally assumed form of the quasi steady wake bubble. Increased blockage is seen to displace the vortex formation region further downstream behind the prism. His tests also included exploratory studies related to hydro-elastic vibrations of bluff bodies under blocked conditions.

Recently Shaw[9,14] has published considerable experimental data on the characteristics of flow past a normal flat plate

and a gate type protrusion placed in the constricted flow passage of a water tunnel. His results indicate that the contraction coefficient C_c as also the drag coefficient C_d for the normal plate model and the gate model tend to approach identical values at blockages which are at least moderate. The discrepancy of the drag coefficient C_D for the gate compared to the C_D of the plate at low blockages is attributed to the deviations in the pressure distribution at the upstream ends caused by the tunnel wall boundary layer. Since C_c is the same for both models and also because the suction at the rear of the body predominates over the pressure force on the front side of the body at higher blockages, the value of C_D for the gate reaches that of the normal plate as the blockage increases. For both cases(at higher blockages), he concludes that:

$$k \cong B/(C_c b_1) \qquad ..(4)$$

using (4), one can write (3) as,

$$u_s/u = B/(C_c b_1) \qquad ..(5)$$

By continuity argument (Fig.1) it is easily infered that,

$$u_j/u = B/(C_c b_1) \qquad ..(6)$$

and as such, this leads to the conclusion that (for higher blockages),

$$u_j = u_s \qquad ..(7)$$

This result will be used in a subsequent section. Observe that the theoretical value of C_c applies equally well to the normal plate and the gate model.

Shaw[14] has also presented the drag coefficients of flat plates set at varying inclinations to the direction of flow.

His test data indicates that the upstream pressure coefficient becomes negligibly small compared to the downstream pressure coefficient for higher blockages of the normal plate. This, naturally leads to higher drag coefficients for confined flows as compared to the unconfined case. His results for normal plates indicate that the measured value of u_j denoting the velocity of the contracted jet at the vena contracta agrees well with the velocity u_s at the separating point for moderate blockages and that C_D varies as the square of (B/b).

Although there has been considerable discussion of the validity of comparison between his tests on normal plates and gates due to the nature of the afterbody configuration, the drag coefficients reported by Shaw for higher blockages are consistent when one notes that boundary layer effects are negligible at larger gate protrusions and that the value of u_j (Fig.1), and hence C_p^* the pressure coefficient at the base, is the same for both cases. The latter is related to the contraction coefficient C_c which is the same (theory) for both cases.

When one considers the flow past the gate, purely from the view point of wake dynamics, it is clear that we do not have interacting shear layers which give rise to the Karman vortex trail as in the case of the normal plate. This does not mean that vortex shedding is not present for flow past gates[24]. Appel[26] provides a useful discussion about the formation of vortices due to sudden expansion associated with flow past protruding objects.

Interference effects on vortex shedding from gates and normal plates have been presented for a range of blockages by Shaw[27]. He used towing tests and visual observations to arrive at the Strouhal numbers for the models which were eccentrically mounted. It was not clear how the wall end was sealed during towing. Even a slight lead can provide pressure communication between the two sides of the model, which will invalidate true gate action.

EXPERIMENTAL SET UP AND PROCEDURES

Tests were conducted in a 14" x 10" test section of the wind tunnel. The models had a nominal height of 10 inches and were made of styrofoam. A coaxial metal tube provided adequate rigidity to the models. The model surfaces were sanded to a smooth finish. Circular cylinders and equilateral triangular prisms of varying widths (Fig.2) were chosen as the basic shapes. They were cantilevered into the test section as shown in Fig.3.

A displacement sensing transducer (Fig.3) was mounted on a force gauge to which the models were attached. The force gauge had a natural frequency of 130 cps and sensed the dynamic forces acting on the bluff bodies subjected to wind loading. For drag measurements the gauge was turned through 90° from the position shown in Fig.3. Steady drag and lift forces were registered for the models only in the range of wind speeds where excessive vibration of the support stand or the models did not occur. When the vortex shedding frequency attained a higher values, the test body was lowered and held rigid against the tunnel floor to avoid vibration. Under these circumstances, vortex shedding was detected in the earlywake of the body with the help of the hot wire anemometry and force measurements were discontinued.

The associated instrumentation is sketched in Fig.4. After filetering, the force signals were recorded on a D.C. digital voltmeter during tests related to steady force coefficients. The frequency of vortex shedding 'f' was generally obtained by recording the unsteady lift force signal on a strip chart recorder. When the frequency of vortex shedding was not quite distinct or when the hot wire was in use, the signals were stored on a Hewlitt-packard magnetic tape recorder and analysed with the help of a B & K wave analyser-level recorder unit.

Other experimental procedures consisted of recording the velocity at the entrance to the test section with the help of a pitot tube-Betz monometer combination. This in turn yielded the undisturbed (mean) velocity u at the plane of the test body. Care was taken to center and align the model axis. The model axis was always within 1/16 inch from the center line of the test section. The orientation of the symmetric shapes were confirmed by noting the absence of any steady lift. This was not possible for the unsymmetric shapes such as the triangular prism set at 30° orientation. Unfortunately, for this orientation of the triangular prism, the steady force and vortex shedding frequency were very sensitive to minor changes in the relative incidence of the air stream. As such, a more elaborate experimental procedure is required to confirm the reported results. Hence, the data for the 30° prism orientation should be viewed as tentative results of an exploratory test program.

ANALYSIS OF RESULTS

Figs. 5 to 14 indicate the present test results related to force coefficients and Figs.15 to 19 denote the test results related to vortex shedding frequencies for flow past the two models which were subjected to wall interference. The various definitions related to data reduction are mentioned briefly in Appendix 1.

A remark related to the use of the gap velocity u_1 and the contracted jet velocity (Fig.1) u_j as scaling factors for the modified steady force coefficients and the Strouhal numbers, is in order. The choice of u_1 and u_j to form C_{D1}, C_{Dj}, S_1 and S_j was based only on simple dimensional considerations. Further, no attempt was made to unify the test results of all the shapes. This is especially true of frequency data, since the dynamics of the flow is more complex and is bound to elude such simple propositions of exchanging velocity scales to

account for blockage effects. For instance, it will be shown that S_j is no longer constant even for a single shape. Also, the Strouhal number S_j for the triangle at 0°, is no longer constant for b/B > 0.3, although C_{Dj} is constant for all the blockages (Figs. 10 & 19).

Steady Force Coefficients:

The steady force coefficients namely C_D and C_L are defined in the usual way using the undisturbed velocity u (Fig.1) for the velocity scale. As expected, there was no detectable Reynolds number effects on C_D for the triangular prisms in the range covered (Figs.5, 6 and 7). The drag coefficient data is replotted in Figs.8, 9 and 10 according to the blockage number. This is defined as the relative model width (b/B or d/B) compared to the test section width B (see Fig.1 and also Appendix).

The values of the drag coefficient C_D steadily increase with blockage for all the three orientations of the triangular prism. For C_D, the normalising velocity was the undisturbed velocity u (Fig.1). Clearly, u did not normalise the values of C_D and provide a constant value of the drag coefficient for any of the orientations of the triangular prism for varying blockages. Therefore, the average gap velocity u_1 (Fig.1) was tried as a substitute in place of u to formulate a new drag coefficient C_{D1}. u_1 reflects the increased velocities in the gap caused by the wall interference. Hence, it accounts in part to the variations in the back pressure C_p^*, which influences the drag force. The drag coefficient so formed by substituting u_1 in place of u was helpful in normalising the drag data and providing a nearly constant value of C_{D1} for the 60° orientation of the triangular prisms for all blockages (Fig.8). The highest blockage b/B was slightly in excess of 70 per cent. On the other hand, for 0° orientation of the prism, C_{D1} still maintained a rising trend with blockage (Fig.10).

As such, further adjustment to the drag data appeared imminent. By substituting the mean contracted jet velocity u_j (Fig.1) in place of u, it was decided to form yet another drag coefficient C_{Dj}. The contracted jet velocity truly reflects the overall effects of the blocked flow in terms of the suction pressure coefficient C_p^* including the variability in the contraction coefficient with blockage. In fact C_{Dj} seems to be the logical choice for the drag coefficient as indicated in Fig.10. It was observed earlier that $u_s = u_j$ for blockages which are at least moderate. Also, under these circumstances, the suction in the rear of the body is the predominant component in determining the effective pressure drag of bluff objects. Since the back pressure $C_p^* = 1-k^2$, it is not surprising that $u_s (=ku)$ and hence u_j effectively normalises the drag force. The variations in C_c for a normal plate computed by Shaw were used in arriving at C_{Dj} for the 0° orientation, since the effect of the afterbody on C_D in the case of the 0° orientation was considered to be only marginal.

The fact that the gap velocity u_1 (Fig.1) itself provides the suitable velocity scale for the drag coefficient C_{D1} of the 60° orientation at all blockages needs some further explanation. This underscores the possibility that, C_c and hence u_j/u_1 is a constant or utmost a slowly varying function for larger blockages. In fact indirectly, there is some qualitative evidence to this effect. For instance the variations of C_c for a range of b/B from 0.2 to 1.0 for a 30° contracting end nozzle is shown to be under 5 per cent[28].

The drag data for the 30° orientation, when plotted as a function of blockage failed to maintain a constant value when the normalisation of drag data was performed using u_1 (Fig.9). In the 30° orientation, the triangular prism has a flow contraction, only on one side. One of the major causes of the variation in C_{D1} could be due to the fact that the drag force is extremely sensitive to the incidence of the flow direction when $\theta = 30°$. This is immediately apparent

from the data presented earlier by Toebes[29] related to the drag force coefficient's variation with prism orientation. This is shown in Fig.11. It was reported that the Strouhal number too was very sensitive to changes in orientation when Θ was set at 30°. It is proposed that these facts could be a result of the shift in the location of one of the separation points, which might move from the front end to the rear end of the model (Fig.1), for a small variation of the flow direction leading to considerable changes in the base pressure and hence the drag force. Slight variations in the orientation of a model can occur due to slight variations in the direction of the incident wind stream in the test section.

Fig.12 indicates the variation of the steady lift coefficient C_L with Reynolds number for the 30° orientation of the triangular prism. As expected, once again there are no noticeable Reynolds number effects. C_L steadily increases with blockage in the grouped data (Fig.13). Replacing u by u_1 to yield C_{L1} as in the drag term renders the data to fall in place and provide a nearly constant value of C_{L1} for the entire blockage range tested. It was not quite apparent why the lift coefficient C_{L1} for all blockages maintained a nearly constant value, although the drag coefficient C_{D1} was still varying with b/B.

The values of C_D for the circular cylinder for various Reynolds numbers at fixed blockages display some sensitivity to Reynolds number R only in the higher Reynolds number range (Fig.14). When the drag data is normalised with u_1, the resulting C_{D1} - R curve maintains a reasonably constant value till the flow around the cylinder attains the critical Reynolds number R_c for a given blockage. For a given blockage, when the critical Reynolds number for the flow is reached, the value of the drag seems to drop down as one would expect. The exact value of R_c of course depends on the characteristics of the free stream turbulence[32], the roughness of the surface and

the blockage. The curves also imply that the critical Reynolds number is reached much earlier when the flow is blocked more. The collapse of the data related to C_{D1} into a single line in the subcritical range implies once again that the contraction coefficient is very insensitive to blockage when the latter is caused by a shape resembling a circular cylinder. The results of Toch[30,31] in the context of determining C_c for sector taintor gates which had a range of exit angles suggests that the contraction coefficient is a very weak function of flow constriction. The trends of C_{D1} shown beyond the critical Reynolds number range for the blocked cylinders in Fig.14 should be viewed only as tentative trends. The amount of data collected in this range is inadequate to advance firm conclusions. For the cylinder set in an unlimited flow[28] C_D is plotted in both the sketches of Fig.14 for comparison with the blocked flow data.

Vortex Shedding Frequency:

The basic vortex shedding frequency f was normalised using the lateral dimension (d or b) of the bodies for the length scale and u for the velocity scale. The resulting Strouhal numbers S for different blockage ratios of triangular prisms and cylinders are plotted as functions of Reynolds number R (Figs.15 and 16). Although there was a systematic increase in the Strouhal number with increased flow constriction, no significant Reynolds number effects were apparent. Unfortunately, the opportunity to collect frequency data in the neighbourhood of R_c was denied due to equipment limitation. For instance, spectral analysis of the low frequency data for larger bodies could not be processed in the wave analyser which had a threshold value of 20 cps at the low end of the spectra. The model mounting mechanism limited the use of very high velocities in the test section as the associated forces were estimated to be prohibitive.

Strouhal number data is regrouped in terms of blockage in Figs.17 and 18. The Strouhal number S continues to increase with blockage for all the model shapes. As before, u was replaced by the gap velocity u_1 (Fig.1) to form a new Strouhal number S_1. Fig.18 indicates that S_1 is constant for a cylinder in the range of blockages tested in the subcritical range. Figs.19(b) and 19(c) indicate that u_1 provides a useful velocity scale to form the Strouhal number S_1 for the 30° and 60° orientations of the prism. It maintains a steady value in the range of blockages tested. Once again, the contracted jet velocity u_j is used in place of u or u_1 to form another Strouhal number S_j for the vortex shedding frequency data of the 0° orientation of the prism. Although S_j is practically constant upto about 27% blockage there is a rising trend for higher blockages, as shown in Fig.19(a).

SUMMARY AND CONCLUSIONS

1. For flow past the two symmetrical triangular prisms and the circular cylinders (subcritical), subjected to moderate or high blockage, experimental evidence shows that the contracted jet velocity u_j ($\simeq u_s$) and the mean gap velocity u_1 provide the proper velocity scales to form the steady drag coefficients C_{Dj} and C_{D1} respectively. When the contraction coefficient C_c does not depend strongly on the degree of blockage, the drag coefficient C_{D1} ($=C_{Dj}/C_c^2$) will maintain a nearly constant value for the specific model shape.

2. Invariance of C_D/k^2 ($=C_{Dj}$) for the three symmetrical shapes implies that u_j ($=u_s=ku$), which denotes a simple increase in the undisturbed velocity u, provides the necessary adjustment to account for the variations in the drag force due to blockage effects. This upholds in part, Maskell's proposition that a simple increase in the velocity may account for the increase of drag in blocked flows. However, based on Shaw's test data it can be asserted that in blocked flows, dynamic similarity cannot be achieved by a mere change in the velocity scale. The degree of accelerations along the forebodies of bluff shapes near the separation points depend on blockage. This in turn, alters the pressure distribution and hence, there is no scope for dynamic similarity.

3. The drag coefficients for circular cylinders in the critical Reynolds number range indicate that increased blockage promotes early transition leading to lower drag forces. This result further shows that Maskell's proposition regarding dynamic similarity for blocked flows breaks down, when boundary layer effects control the location of the separation point.

4. Tentatively, it can be stated that the steady lift force for the unsymmetric triangle ($\theta = 30°$) when normalised by the gap velocity u_1 yields a nearly constant lift coefficient, C_{L1}.

5. The vortex shedding frequency and the body size together with the gap velocity u_1 provide a nearly constant values for the Strouhal numbers S_1 for the circular cylinders (subcritical flow) and the triangular prisms at the 30° and 60° orientations. Although the use of u_j was effective in yielding a proper velocity scale for the Strouhal number S_j for the prism at 0° orientation upto blockages of 0.3, S_j seems to increase beyond this blockage. This confirms the earlier findings of Toebes[12].

SCOPE FOR FURTHER STUDIES AND APPLICATIONS

It was observed that wall interference to flow past a single body was qualitatively similar to the interference of neighbouring cylinders on each other in multiple body configurations, especially when the boundary layer effects are not excessive and one restricts the attention to steady forces. As such the use of u_1 and u_j to normalise steady force coefficients of multiple bodies may be studied. These configurations are of considerable interest in practice[33,34]. In this regard, partial groups of bodies (Fig.26) can be studied as single bodies set eccentrically between bounding walls. The force and frequency study can be extended to flexible structures, which are subject to blockages. Here hydroelastic effects[35,36,37] should be included.

The results of the studies reported and proposed have practical applications in the following areas:

1. Forces on Single Buildings and Groups of Buildings due to wind.
2. Vibration of Heat Exchanger tubes due to gas stream.
3. Forces on ocean piles and bridge piers.
4. Power computations of air ducts fitted with oversize obstructions.
5. Transferring model data to prototype design information.

APPENDIX 1

APPENDIX 1

Some Definitions

The scales chosen for the length and velocity for purposes of data reduction are included below.

Blockage is defined as the ratio of the largest lateral model dimension (d for the circles and b for the prisms - Fig.3) to the tunnel width B.

The Reynolds number R is formed using the same model dimension. Thus,

for circles, $R = ud/\nu$ ..(8)

for triangles, $R = ub/\nu$ ..(9)

Three types of drag coefficients are defined namely C_D, C_{D1} and C_{Dj}. The only distinction between the three is the choice of the velocity scale chosen for non-dimensionalising the steady force.

Thus, C_D for the triangular prism denotes the usual definition of the drag coefficient:

$$C_D = \text{steady drag force} / \tfrac{1}{2} \rho u^2 bL \quad ..(10)$$

where,

ρ = the density of air, bL = area of any one of the prism faces.

The velocity scales, u_1 and u_j (Fig.3) are used to define C_{D1} and C_{Dj}:

$$C_{D1} = \frac{\text{Steady drag force}}{\frac{1}{2} \rho u_1^2 bL} = C_D(u/u_1)^2 \quad ..(11)$$

$$C_{Dj} = \frac{\text{steady drag force}}{\frac{1}{2}\rho u_j^2 bL} = C_D(u/u_j)^2 \quad ..(12)$$

where (from Fig.1), $u_1 = uB/b_1$ ..(13)

and $$u_j = \frac{uB}{(B - b')} = \frac{uB}{b_1 C_c} \quad ..(14)$$

Since, $u_j = u_s$ (velocity at separation) $=ku$, when blockage exceeds a certain minimum value, one can write $C_{Dj} = C_D/k^2$. Equations (13) and (14) follow from continuity arguments.

Similar relations hold good for the steady lift coefficients C_L, C_{L1} and C_{Lj} and the Strouhal numbers S, S_1 and S_j.

Thus,

$$C_L = \frac{\text{steady lift force}}{\frac{1}{2}\rho u^2 bL} \quad ..(15)$$

$$C_{L1} = C_L (u/u_1)^2 \quad ..(16)$$

and $$C_{Lj} = C_L (u/u_j)^2 = C_L/k^2 \quad ..(17)$$

The Strouhal numbers are defined as:

$$S = fb/u \quad ..(18)$$

$$S_1 = fb/u_1 \quad ..(19)$$

$$S_j = fb/u_j = S/k \quad ..(20)$$

The so-called universal Strouhal number defined by Roshko[16] is given by the expression:

$$S^* = \frac{fb'}{u_s} \qquad ..(21)$$

For blockages, which are at least moderate, $u_s = u_j$ and $B = b' + C_c b_1$ from Fig.1. Hence, S* can be expressed as:

$$S^* = \frac{f(B - C_c b_1)}{u_j} \qquad ..(22)$$

APPENDIX 2

B I B L I O G R A P H Y

1. A.B. Putnam: FLOW INDUCED NOISE AND VIBRATION IN HEAT EXCHANGERS, ASME Paper 64-WA/HT-21, 1964.

2. B.W. Roberts: THE STUDY FLOW THROUGH A CASCADE OF CLOSELY SPACED CIRCULAR CYLINDERS, J. Roy. Aero. Soc., Vol.70, pp.886-887, 1966.

3. J.L. Livesey and R.C.F. Dye: VORTEX EXCITED VIBRATION OF A HEAT EXCHANGER TUBE ROW, J. Mech. Engg. Sci., Vol.4, pp.349-352, 1962.

4. A.D.K. Laird and W. Warren: GROUP OF VERTICAL CYLINDERS OSCILLATING IN WATER, J. Engg. Mechs. Div., proc. ASCE, Vol.98, pp.25-35, 1963.

5. T. Hsieh: RESISTANCE OF CYLINDRICAL PIERS IN OPEN CHANNEL FLOW, J. Hyd. Div., proc. ASCE, vol.90, pp.161-173, 1964.

6. H. Glauret: WIND TUNNEL INTERFERENCE OF WINGS, BODIES AND AIR SCREWS, A.R.C., R & M 1566, 1933.

7. E.C. Maskell: A THEORY OF BLOCKAGE EFFECTS ON BLUFF BODIES AND STALLED WINGS IN A CLOSED WIND TUNNEL, A.R.C., R & M 3400, 1957.

8. R. Fail, et al: LOW SPEED EXPERIMENTS ON THE WAKE CHARACTERISTICS OF FLAT PLATES NORMAL TO AN AIR STREAM, A.R.C., R & M 3120, 1957.

9. T.L. Shaw: STEADY FLOW PAST FLAT PLATE IN CHANNEL, J. Hyd. Div., proc. ASCE, Vol.95, pp.2013-2018, 1969.

10. V.J. Modi and S. El-Sherbiny: EFFECT OF WALL CONFINEMENT ON AERODYNAMICS OF STATIONARY CIRCULAR CYLINDER, proc. Intl. Conf. on Wind Effects on Buildings and Structures, Tokyo, pp. II 19-1 to II 19-12, 1971.

11. G.H. Toebes: THE FREQUENCY OF OSCILLATORY FORCES ACTING ON BLUFF CYLINDERS IN CONSTRICTED PASSAGES, proc. 14th Congress of Intl. Hyd. Rsch., Vol.2, pp.B-7-49 to B-7-58, Paris, 1971.

12. G.H. Toebes and A.S. Ramamurthy: LIFT AND STROUHAL FREQUENCY FOR BLUFF SHAPES IN CONSTRICTED PASSAGES, proc. Conf. on Flow induced vibration in nuclear reactors, Agronne Natl. Lab., pp.225-247, Illinois, 1970.

13. T. Sarpakya: DISCUSSION ON BUTTERFLY VALVE FLOW CHARACTERISTICS, J. Hyd. Div., proc. ASCE, Vol.B3, pp.(1348) 31-47, 1957.

14. T.L. Shaw: EFFECT OF SIDE WALLS ON FLOW PAST BLUFF BODIES, J. Hyd. Div., proc. ASCE, Vol.97, pp.65-79, 1971.

15. J.M. Robertson: HYDRODYNAMICS IN THEORY AND APPLICATION, Prentice Hall, N.J., 1965.

16. A. Roshko: A NEW HODOGRAPH FOR FREE STREAMLINE THEORY, NACA, TN 3168, 1954.

17. F.H. Abernathy: FLOW OVER AN INCLINED PLATE, Ph.D. Thesis, Div. of Appl. Physics, Harvard Univ., Mass., 1958.

18. A. Tozkas: EFFECT OF CONFINING WALLS ON THE PERIODIC WAKE OF CYLINDERS AND PLATES, M.S. Thesis, Dept. of Engg. Mechs. and Hydraulics, Univ. of Iowa, 1965.

19. Y.S. Chen: EFFECT OF CONFINING WALLS ON THE PERIODIC WAKE OF 90° WEDGES, Dept. of Engg. Mechs. and Hydraulics, Univ. of Iowa, 1967.

20. F.B. Campbell: VIBRATION PROBLEMS IN HYDRAULIC STRUCTURES, Trans. ASCE, Vol.127, part 1, pp.1-17, 1962.

21. C.A.C. Lin: EFFECT OF CHANNEL WALLS ON BASE PRESSURE AND FLOW ABOUT A BLUNT BODY, M.S. Thesis, Dept. of Engg. Mechs. and Hydraulics, Univ. of Iowa, 1966.

22. C.A.C. Lin: A FREE STREAMLINE MODEL OF A TWO DIMENSIONAL WAKE, Ph.D. Thesis, Dept. of Engg. Mechs. and Hydraulics, Univ. of Iowa, 1970.

23. E. Achenback: INVESTIGATIONS ON THE FLOW AROUND A SPHERE IN AN AIR STREAM INVOLVING BLOCKAGE RATIOS UPTO 0.90, Presented at the European Mechanics Colloguium No.17, Cambridge, U.K., 1970.

24. K. Cecen, et al: FORCES DUE TO CYLINDERS FALLING THROUGH WATER IN A VERTICAL TUBE, proc. 14th Congress of Intl. Assn. of Hyd. Rsch., Vol.2, pp.17-24, Paris, 1971.

25. R.J. McKeon and W.H. Melbourne: WIND TUNNEL BLOCKAGE EFFECTS AND DRAG ON BLUFF BODIES IN A ROUGH WALL BOUNDARY LAYER, proc. Intl. Conf. on Wind Effects on Buildings and Structures, Tokyo, pp.II-9, 1.10, 1971.

26. D.W. Appel: Discussion on VIBRATION PROBLEMS IN HYDRAULIC STRUCTURES, J. Hyd. Div., Trans. ASCE, Vol.127, part I, pp.19-24, 1962.

27. T.L. Shaw: WAKE DYNAMICS OF TWO DIMENSIONAL STRUCTURES IN CONFINED FLOWS, proc. 14th Congress of Intl. Assn. of Hyd. Rsch., Vol.2, pp.41-48, Paris, 1971.

28. J.W. Daily and D.R.F. Harleman: FLUID DYNAMICS, Addison Wesley Co., Mass, 1966.

29. G.H. Toebes and A.S. Ramamurthy: ENERGY TRANSFER CHARACTERISTICS OF TRIANGULAR CYLINDERS, presented at the ASCE Struc. Engg. Conf., Kentucky, 1969.

30. F.M. Henderson: OPEN CHANNEL FLOW, Mcmillan Co., N.Y., 1966.

31. A. Toch: DISCHARGE CHARACTERISTICS OF TAINTER GATES, Trans. ASCE, Vol.120, p.290, 1955.

32. S.C. Ko and W.H. Graff: DRAG COEFFICIENT AND TURBULENCE CHARACTERISTICS, proc. 14th Congress of Intl. ASSn. of Hyd. Rsch., Vol.2, pp.33-39, Paris, 1971

33. R.E. Nece and R.D. Unrue: Discussion on RESISTANCE OF CYLINDRICAL PIERS IN OPEN CHANNEL FLOW, J. Hyd. Div., proc. ASCE, Vol.90, pp.223-228, 1964.

34. A.R.J. Borges: VORTEX SHEDDING FREQUENCIES OF THE FLOW THROUGH TWO-ROW BANKS OF TUBES, J. Mech. Engg. Sci., Vol.5, No.5, pp.498-502, 1969.

35. G.H. Toebes: FLUIDELASTICITY, proc. 11th Congress of Intl. Assn. of Hyd. Rsch., Leningrad, Paper No. 4.10, 1965.

36. G.H. Toebes and A.S. Ramamurthy: FLUIDELASTIC FORCES ON CIRCULAR CYLINDERS, J. Engg. Mechs., proc. ASCE, Vol.92 pp.1-2-, 1967.

37. A.Protos, et al: HYDROELASTIC FORCES ON BLUFF CYLINDERS, ASME Paper No. 68-FE-12, 1968.

38. A. Fage and F.C. Johansen: THE STRUCTURE OF THE VORTEX SHEETS, A.R.C., R & M 1143, 1927.

39. P.W. Bearman: ON VORTEX STREET WAKES, J. Fl. Mechs., Vol.28, Part 4, pp.625-641, 1967.

40. Y.N. Chen: FLUCTUATING LIFT FORCES OF THE KARMAN VORTEX STREETS ON SINGLE CIRCULAR CYLINDERS AND IN TUBE BUNDLES, ASME Paper No. 71-Vibr-11, 1971.

41. B.J. Vickery; FLUCTUATING LIFT AND DRAG ON A LONG CYLINDER OF SQUARE CROSS SECTION IN A SMOOTH AND IN A TURBULENT STREAM, J. Fl. Mechs, Vol.25, Part 3, pp.481-494, 1966.

APPENDIX 3

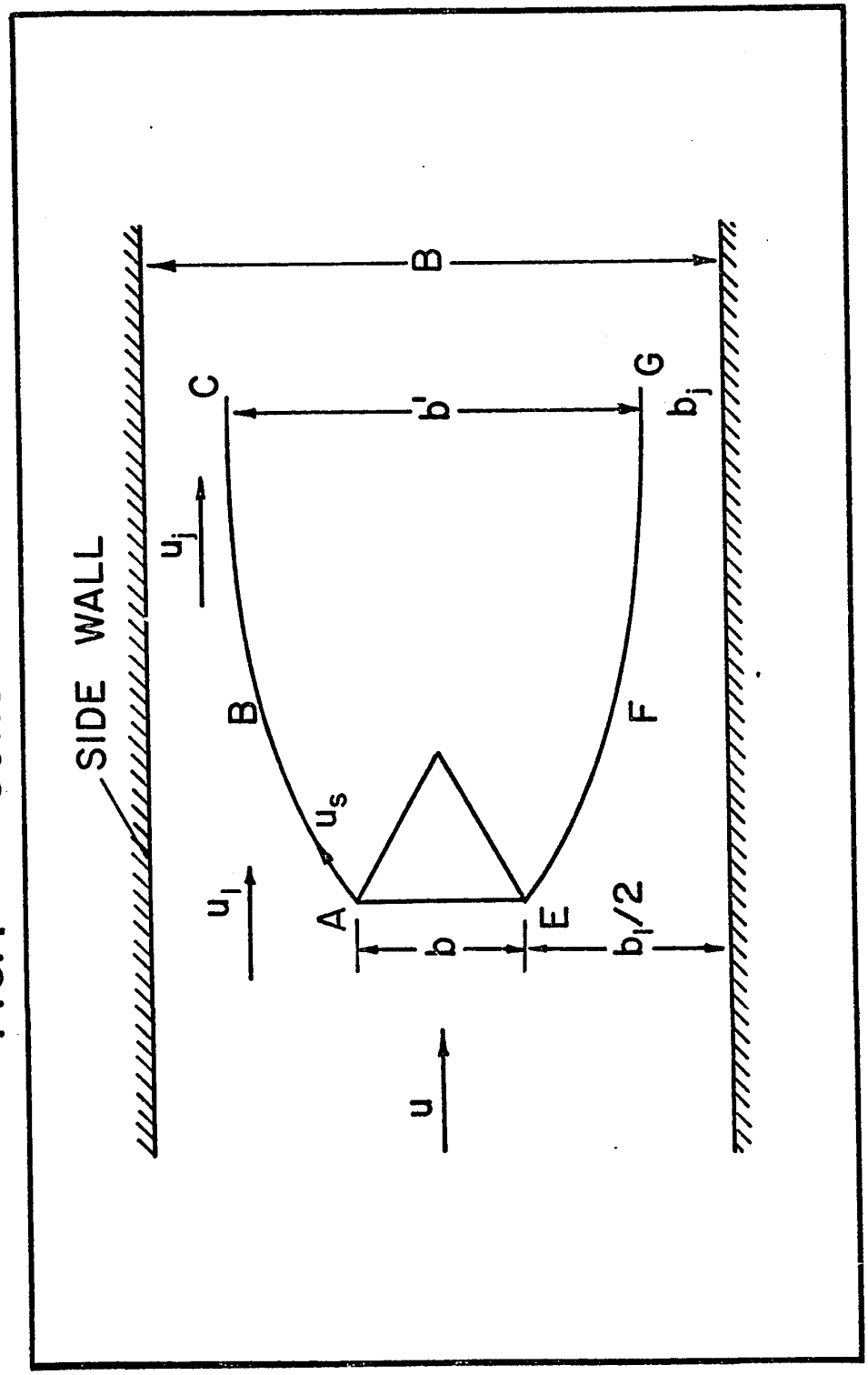

FIG. 1 CONSTRICTED FLOW

FIG. 2 PARAMETER RANGE

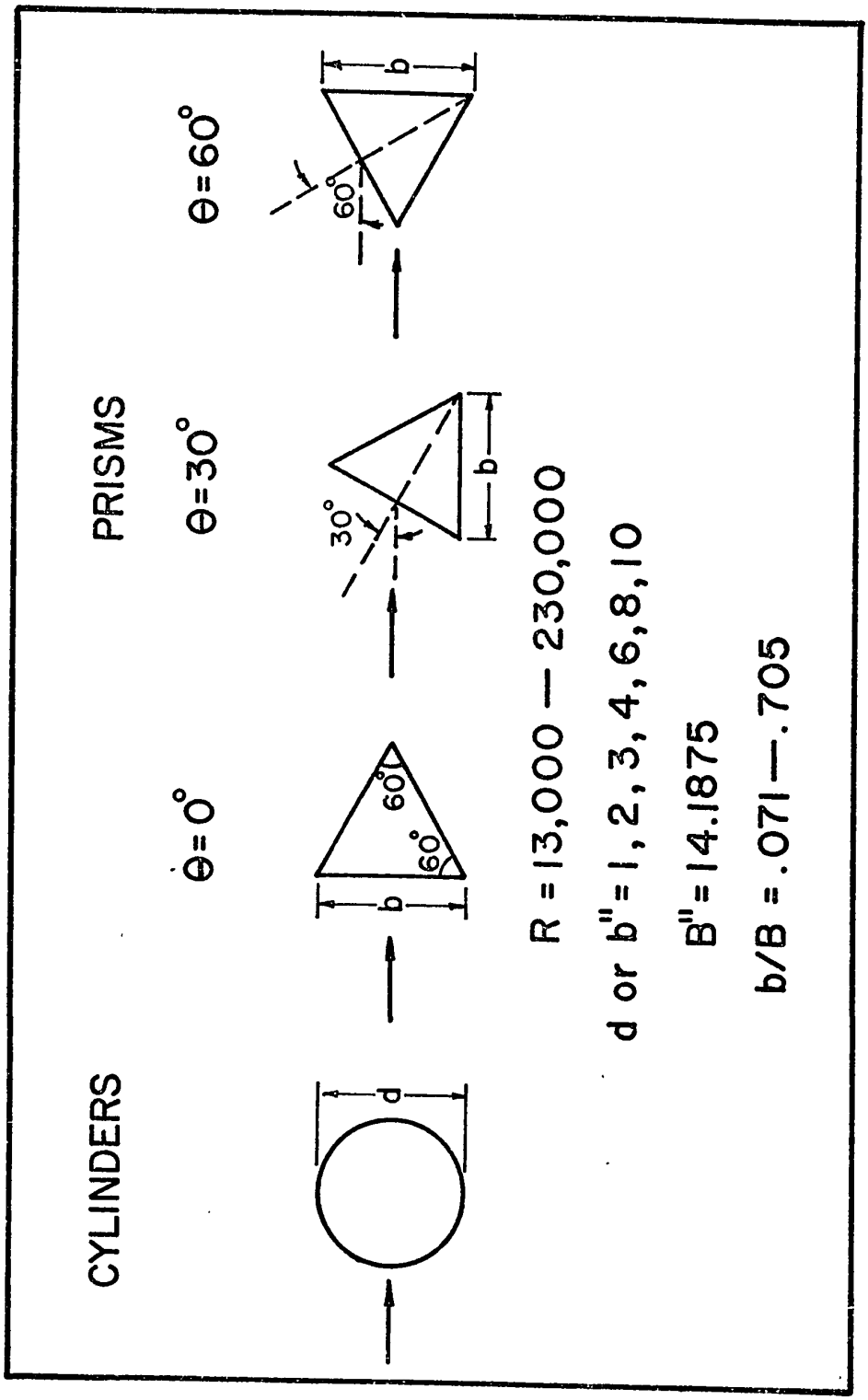

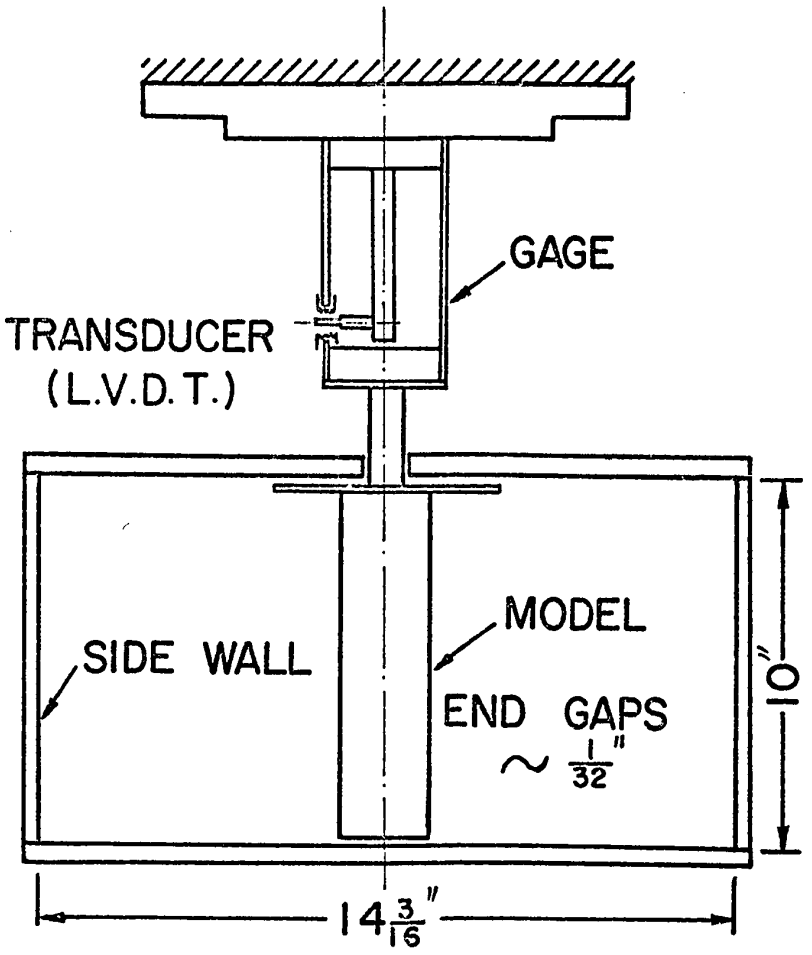

FIG. 3 TEST SECTION

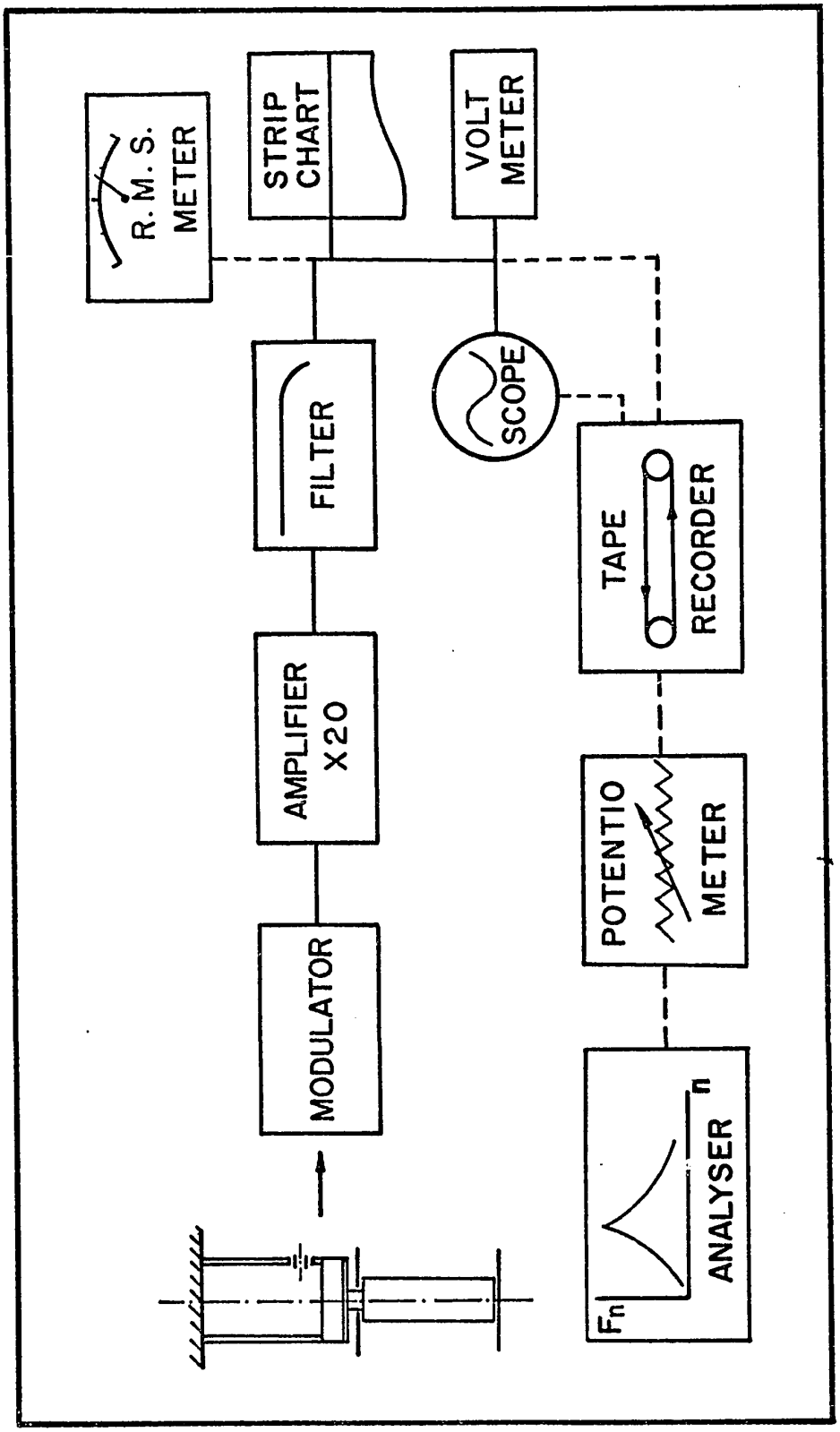

FIG. 4 INSTRUMENTATION

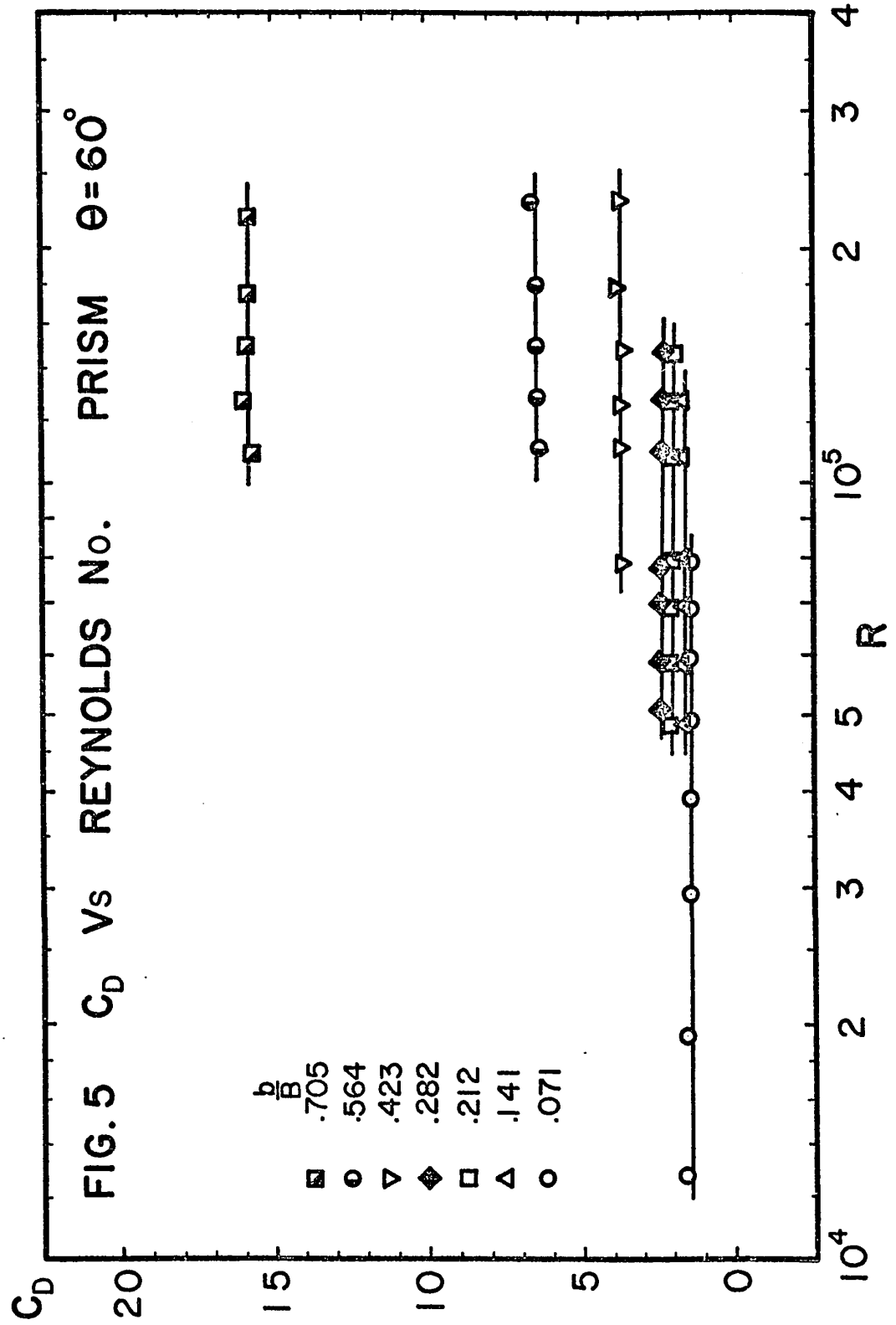
FIG. 5 C_D Vs REYNOLDS No. PRISM θ=60°
C_D
20
15
10
5
0
10^4
2
3
4
5
10^5
2
3
4
R
b/B
.705
.564
.423
.282
.212
.141
.071

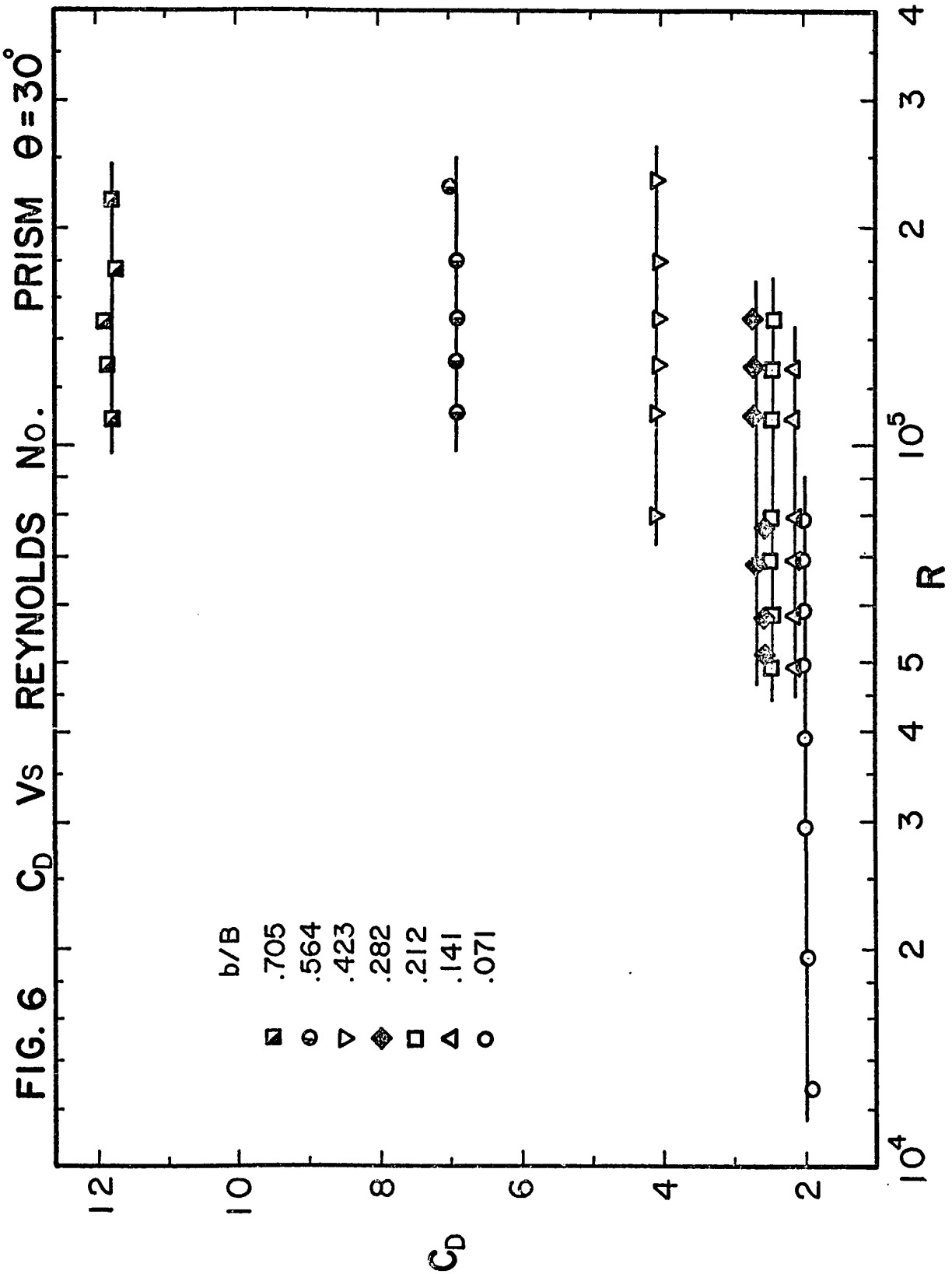
FIG. 6 C_D Vs REYNOLDS No. PRISM θ=30°
b/B
.705
.564
.423
.282
.212
.141
.071
C_D
12
10
8
6
4
2
10^4
2
3
4
5
10^5
2
3
4
R

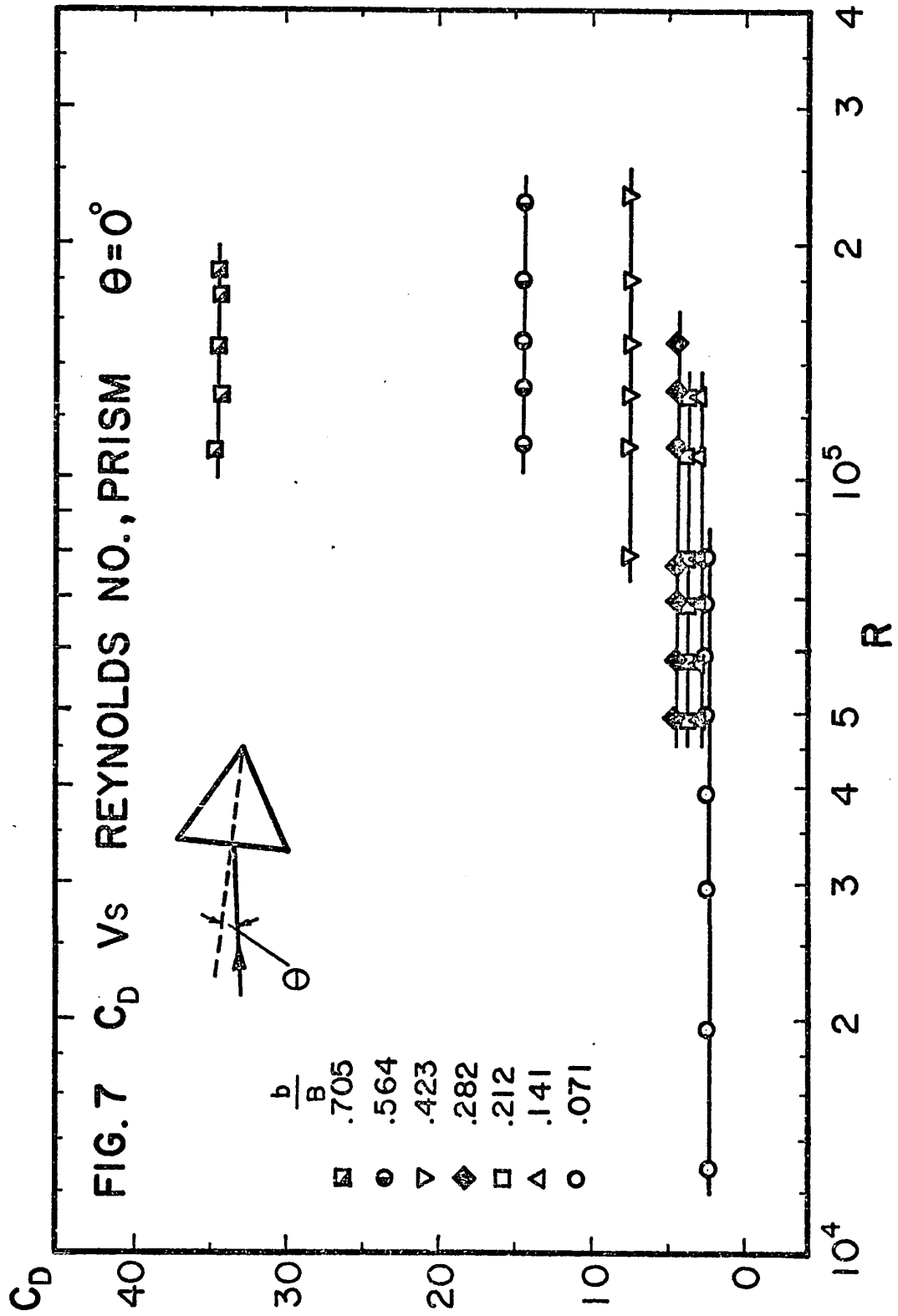
FIG. 7 C_D Vs REYNOLDS NO., PRISM θ=0°
C_D
40
30
20
10
0
10^4
2
3
4
5
10^5
2
3
4
R
θ
b/B
.705
.564
.423
.282
.212
.141
.071

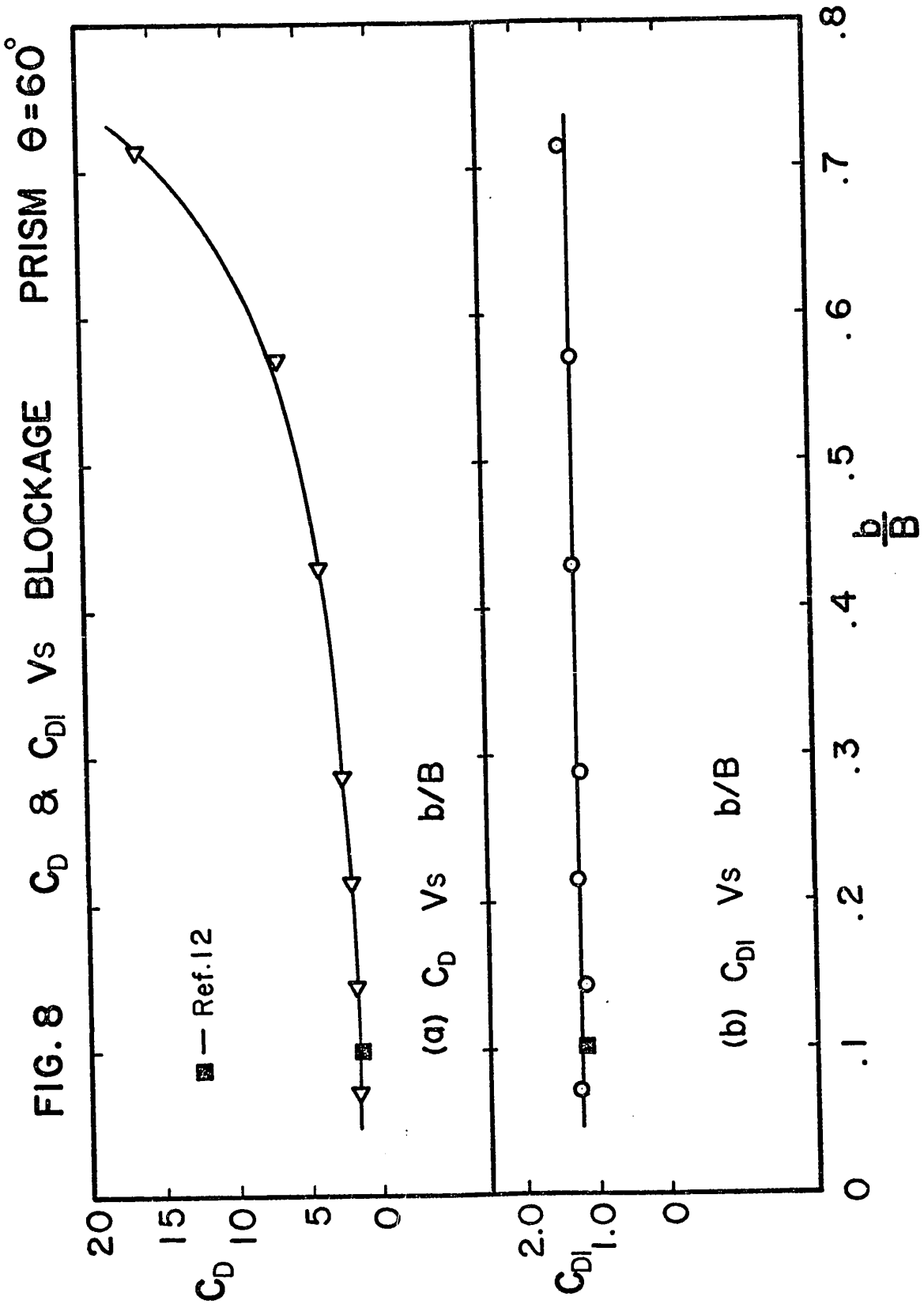
FIG. 8 C_D & C_{DI} Vs BLOCKAGE PRISM θ=60°
■ — Ref.12
(a) C_D Vs b/B
(b) C_{DI} Vs b/B
C_D
C_{DI}
b/B
0
.1
.2
.3
.4
.5
.6
.7
.8
5
10
15
20
1.0
2.0

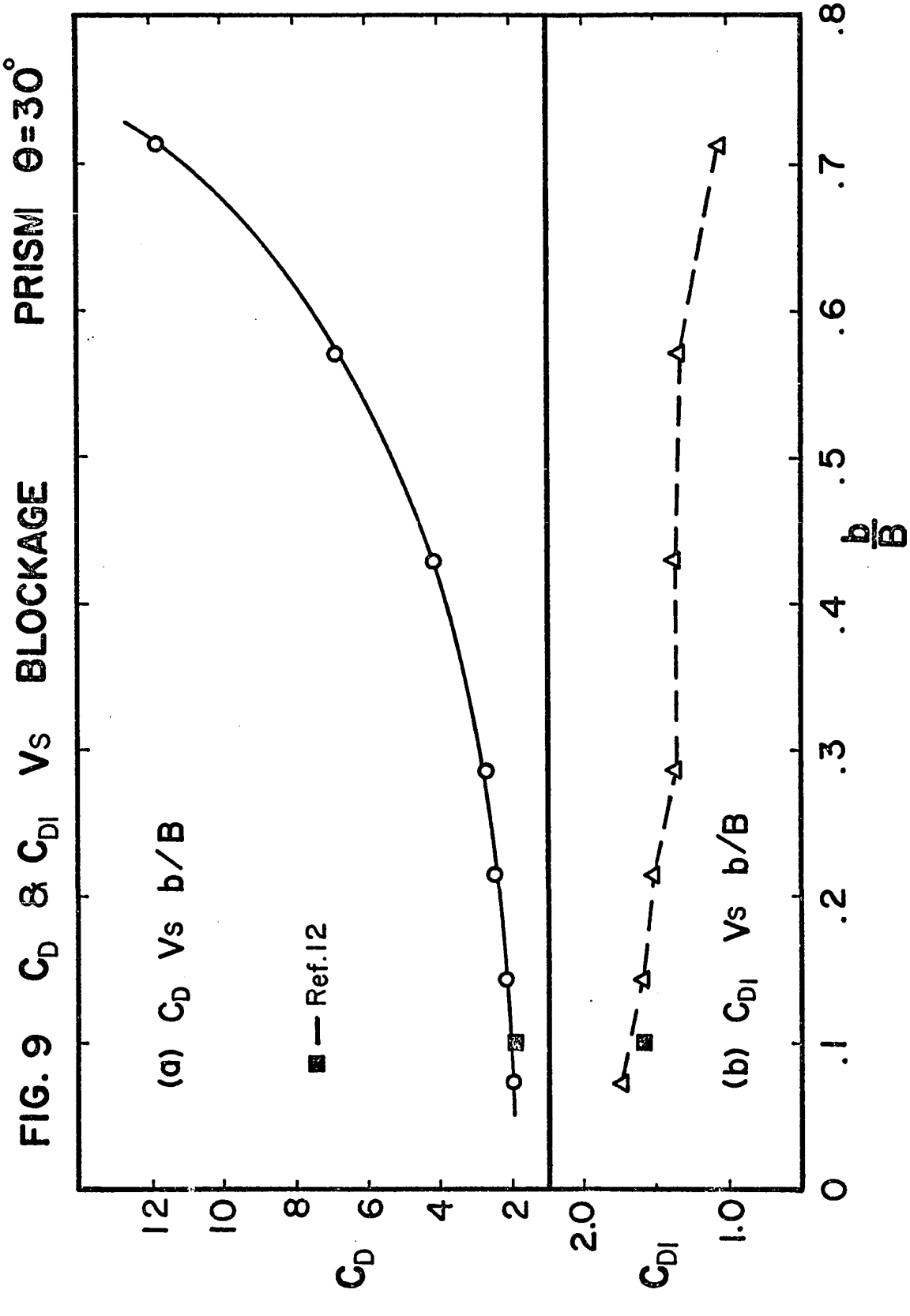
FIG. 9 C_D & C_{DI} Vs BLOCKAGE PRISM θ=30°
(a) C_D Vs b/B
Ref. 12
(b) C_{DI} Vs b/B
C_D
C_{DI}
12
10
8
6
4
2
2.0
1.0
0
.1
.2
.3
.4
.5
.6
.7
.8
$\frac{b}{B}$

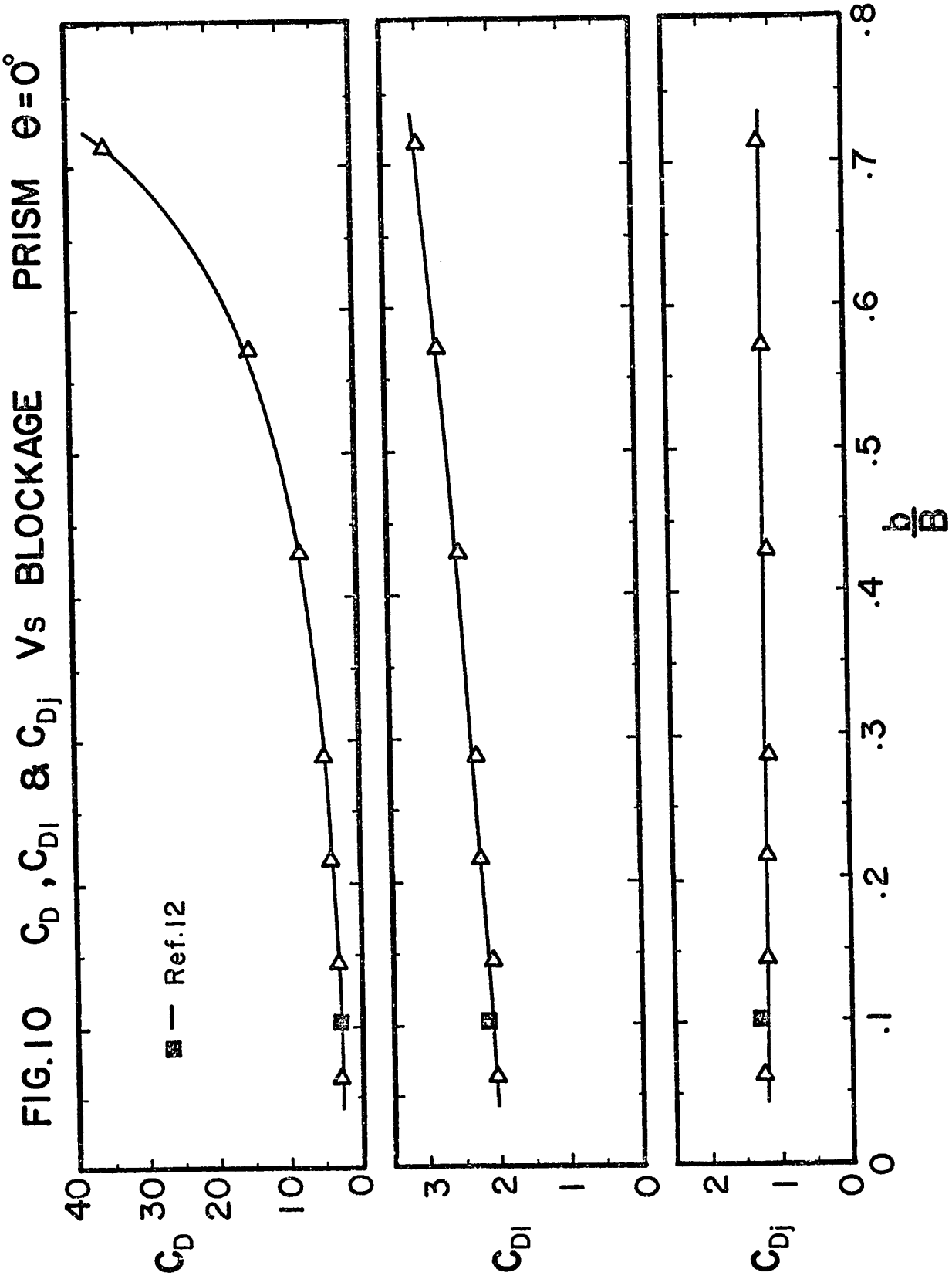
FIG.10 C_D, C_{DI} & C_{Dj} Vs BLOCKAGE PRISM $\theta=0^\circ$
■ — Ref.12
C_D
C_{DI}
C_{Dj}
$\frac{b}{B}$
0
.1
.2
.3
.4
.5
.6
.7
.8
10
20
30
40
1
2
3

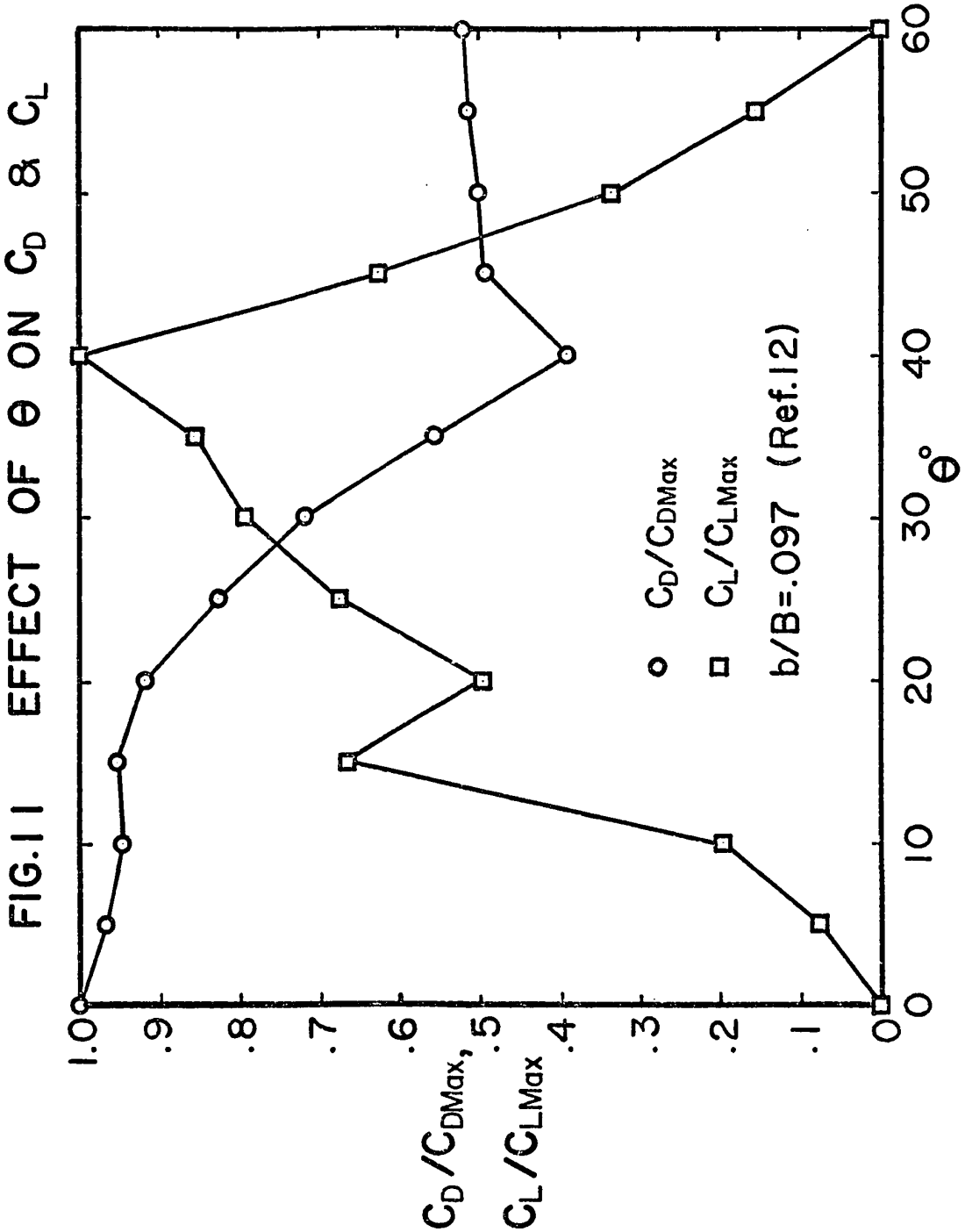
FIG.11 EFFECT OF Θ ON C_D & C_L
C_D/C_{DMax}, C_L/C_{LMax}
1.0
.9
.8
.7
.6
.5
.4
.3
.2
.1
0
0
10
20
30
40
50
60
Θ°
C_D/C_{DMax}
C_L/C_{LMax}
b/B=.097 (Ref.12)

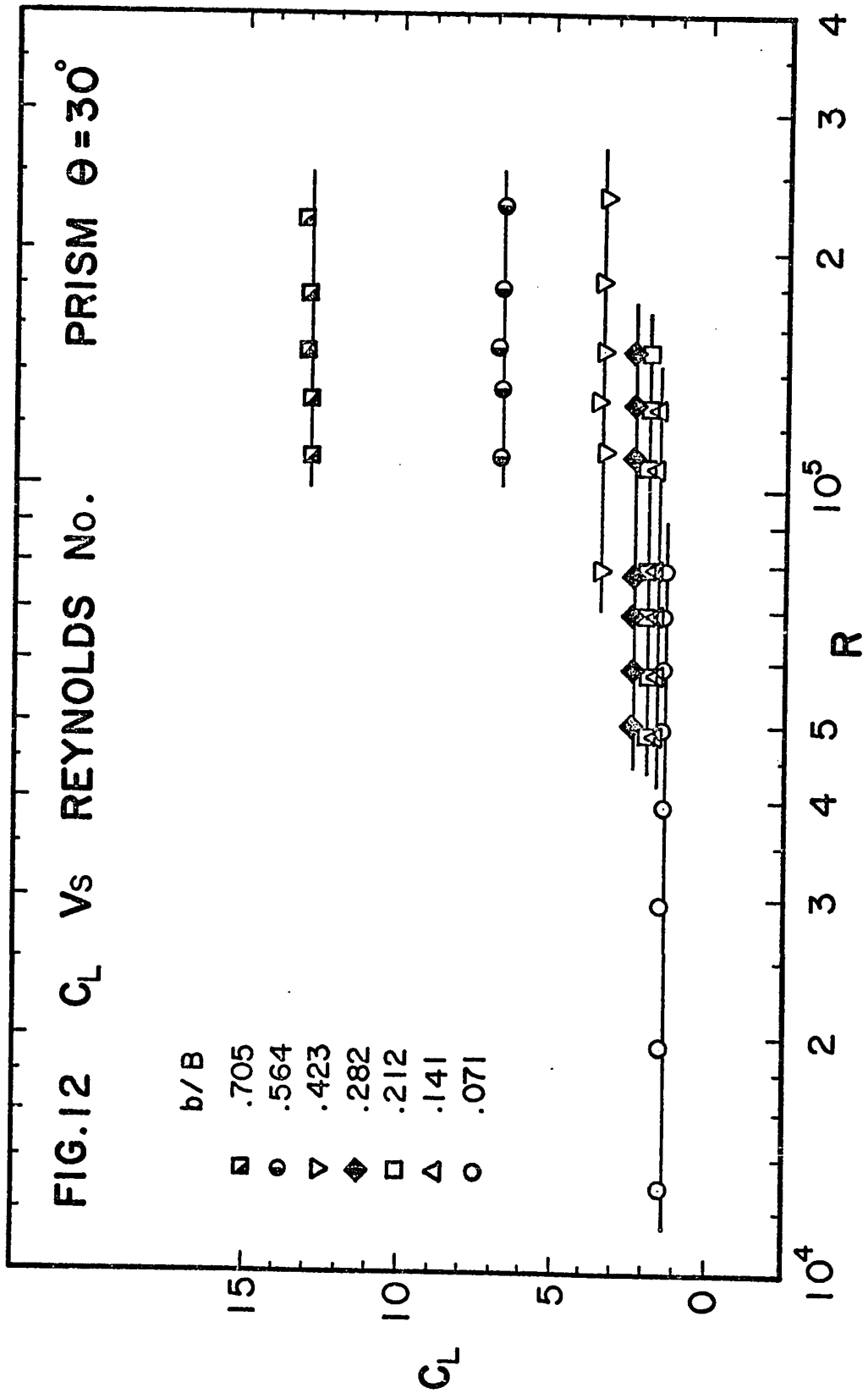
FIG. 12 C_L Vs REYNOLDS No. PRISM Θ=30°
b/B
.705
.564
.423
.282
.212
.141
.071
C_L
15
10
5
0
10^4
2
3
4
5
R
10^5
2
3
4

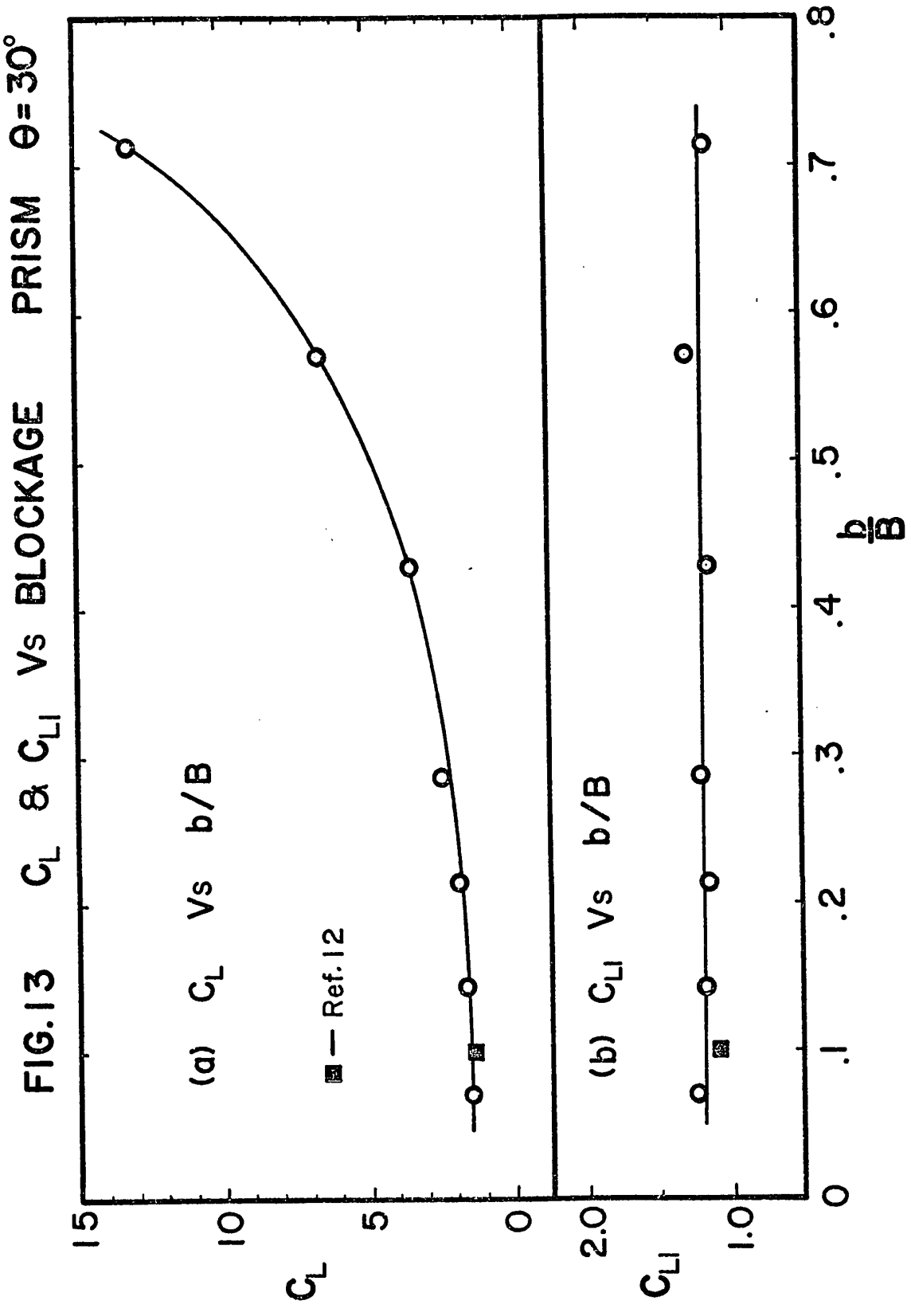
FIG. 13 C_L & C_{LI} Vs BLOCKAGE PRISM θ=30°
(a) C_L Vs b/B
■ — Ref. 12
(b) C_{LI} Vs b/B
C_L
C_{LI}
15
10
5
0
2.0
1.0
0
.1
.2
.3
.4
.5
.6
.7
.8
$\frac{b}{B}$

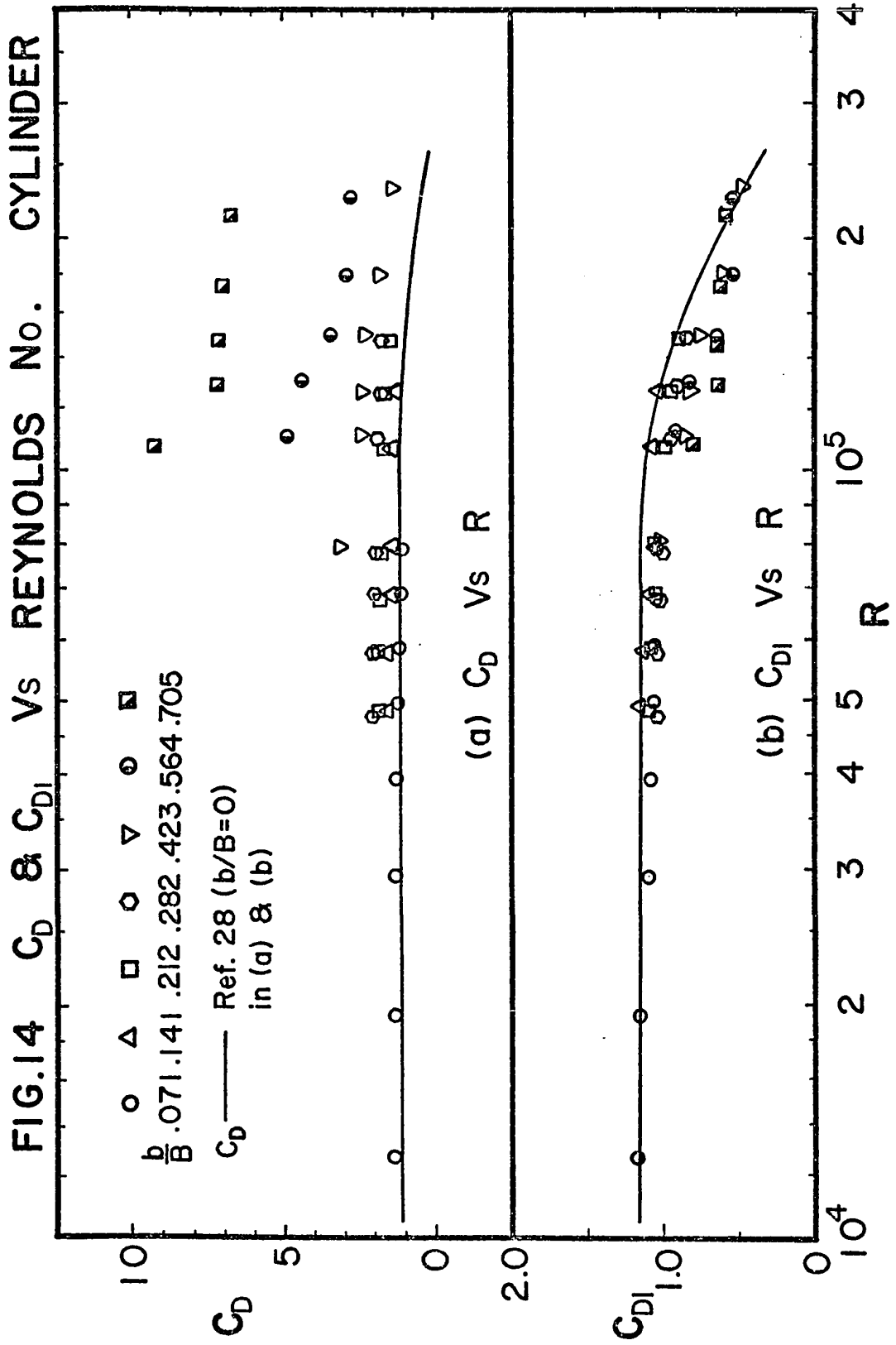
FIG.14 C_D & C_{DI} Vs REYNOLDS No. CYLINDER
b/B .071 .141 .212 .282 .423 .564 .705
C_D —— Ref. 28 (b/B=0) in (a) & (b)
(a) C_D Vs R
(b) C_{DI} Vs R
C_D
C_{DI}
R
10
5
0
2.0
1.0
0
10^4
2
3
4
5
10^5
2
3
4

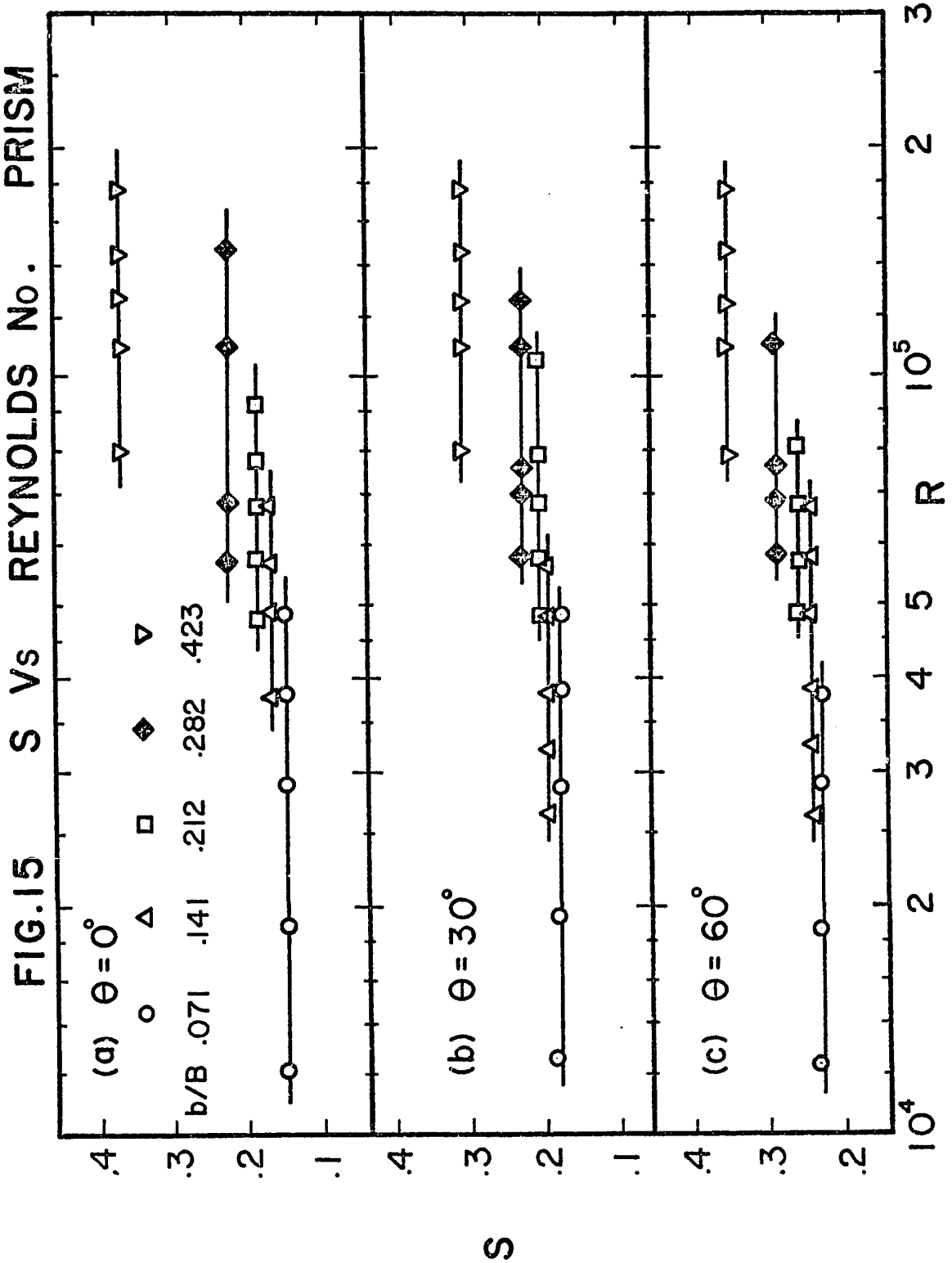
FIG.15 S Vs REYNOLDS No. PRISM
(a) Θ=0°
(b) Θ=30°
(c) Θ=60°
b/B .071 .141 .212 .282 .423
S
R
.4
.3
.2
.1
10⁴
2
3
4
5
10⁵

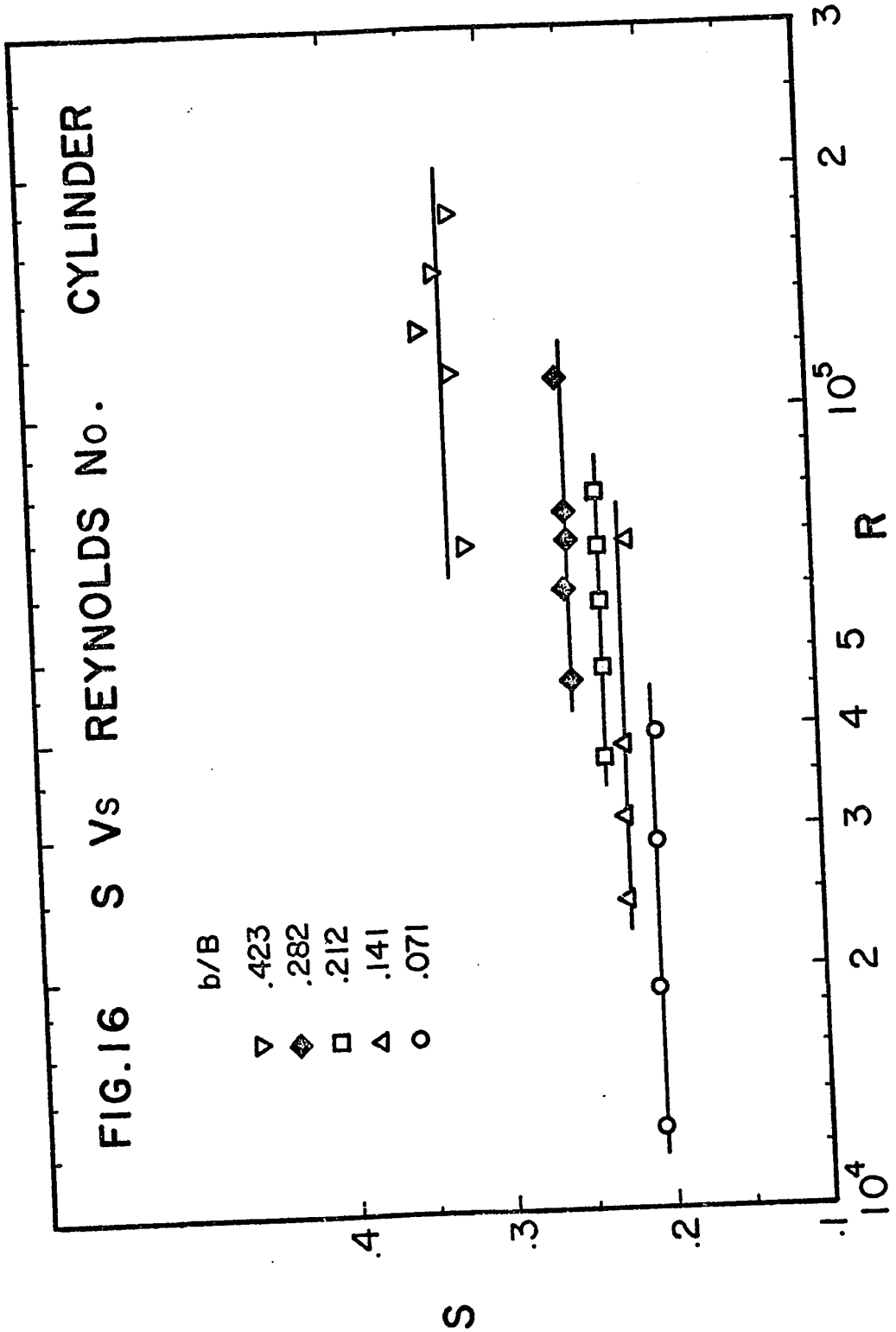
FIG.16 S Vs REYNOLDS No. CYLINDER
b/B
.423
.282
.212
.141
.071
S
.4
.3
.2
.1
10^4
2
3
4
5
R
10^5
2
3

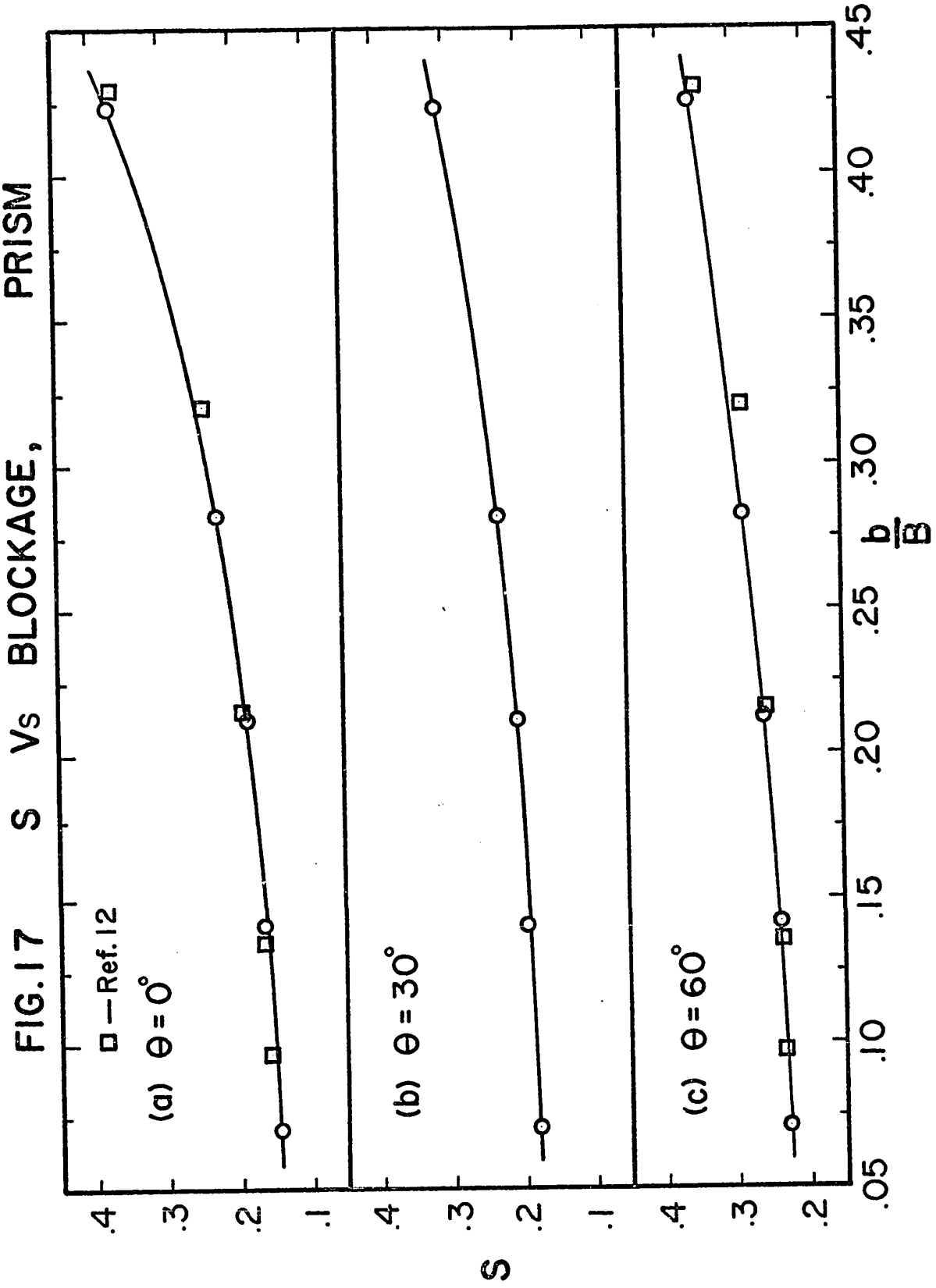
FIG. 17 S Vs BLOCKAGE, PRISM
□—Ref. 12
(a) Θ=0°
(b) Θ=30°
(c) Θ=60°
S
b/B
.4
.3
.2
.1
.05
.10
.15
.20
.25
.30
.35
.40
.45

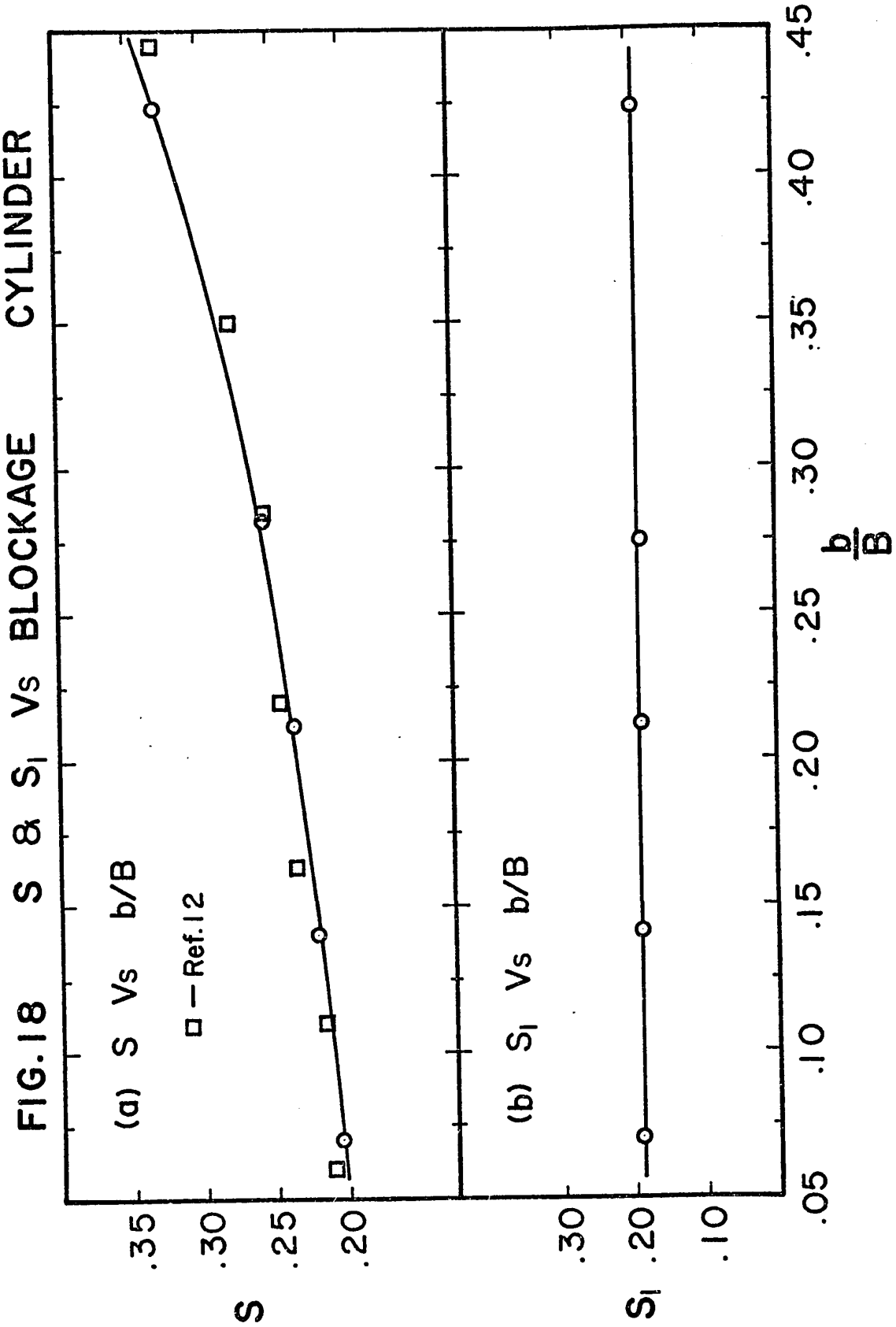
FIG. 18 S & S_I Vs BLOCKAGE CYLINDER
(a) S Vs b/B
□ — Ref. 12
(b) S_I Vs b/B
S
S_I
.35
.30
.25
.20
.30
.20
.10
.05
.10
.15
.20
.25
.30
.35
.40
.45
$\frac{b}{B}$

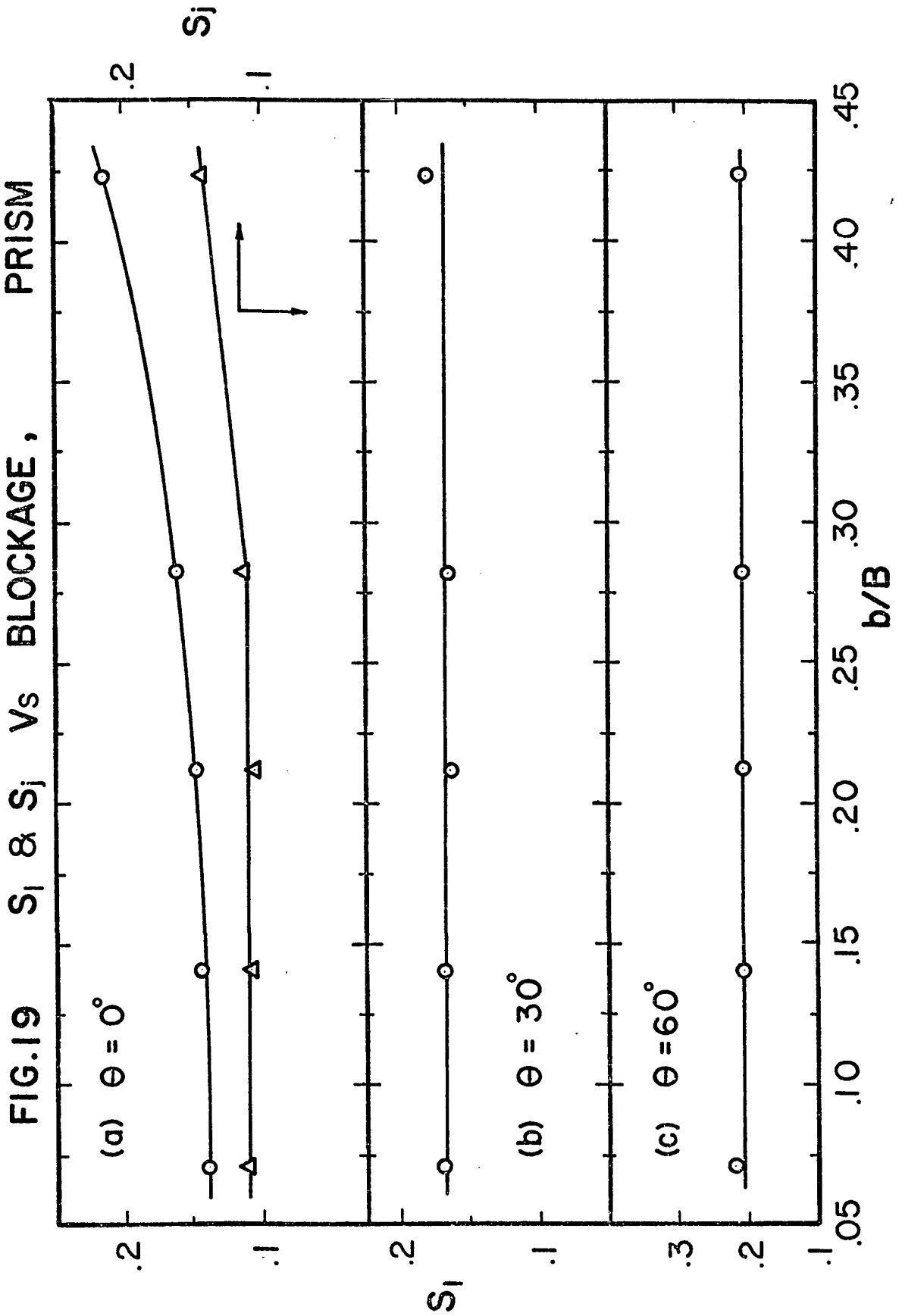
FIG.19 S_I & S_j Vs BLOCKAGE, PRISM
S_j
S_I
b/B
(a) Θ = 0°
(b) Θ = 30°
(c) Θ = 60°

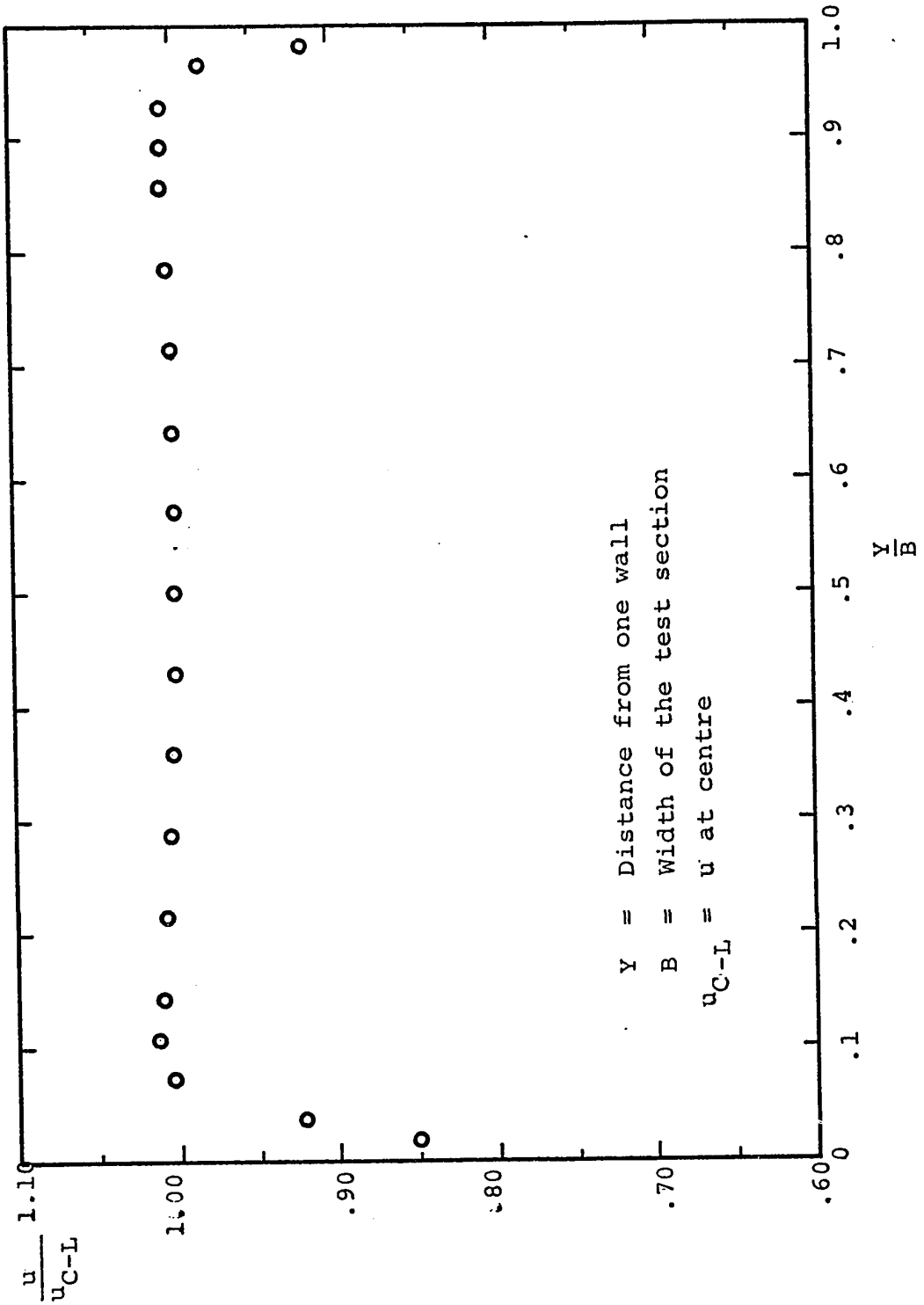

Fig.20 VELOCITY DISTRIBUTION AT THE TEST SEC. (u_{C-L}=69.8 fps)

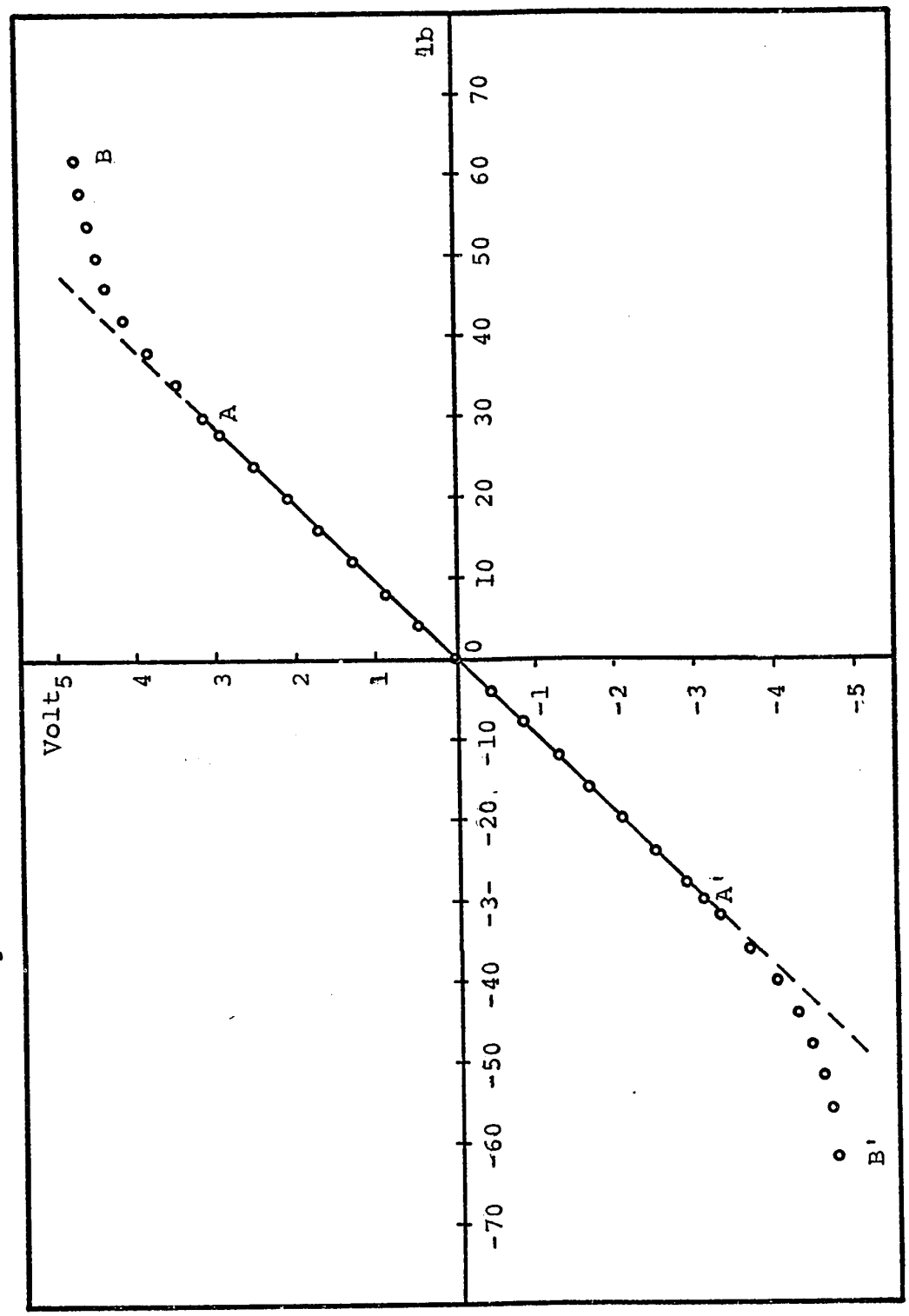

Fig.21 TRANSDUCER CALIBRATION, Volt vs. lb.

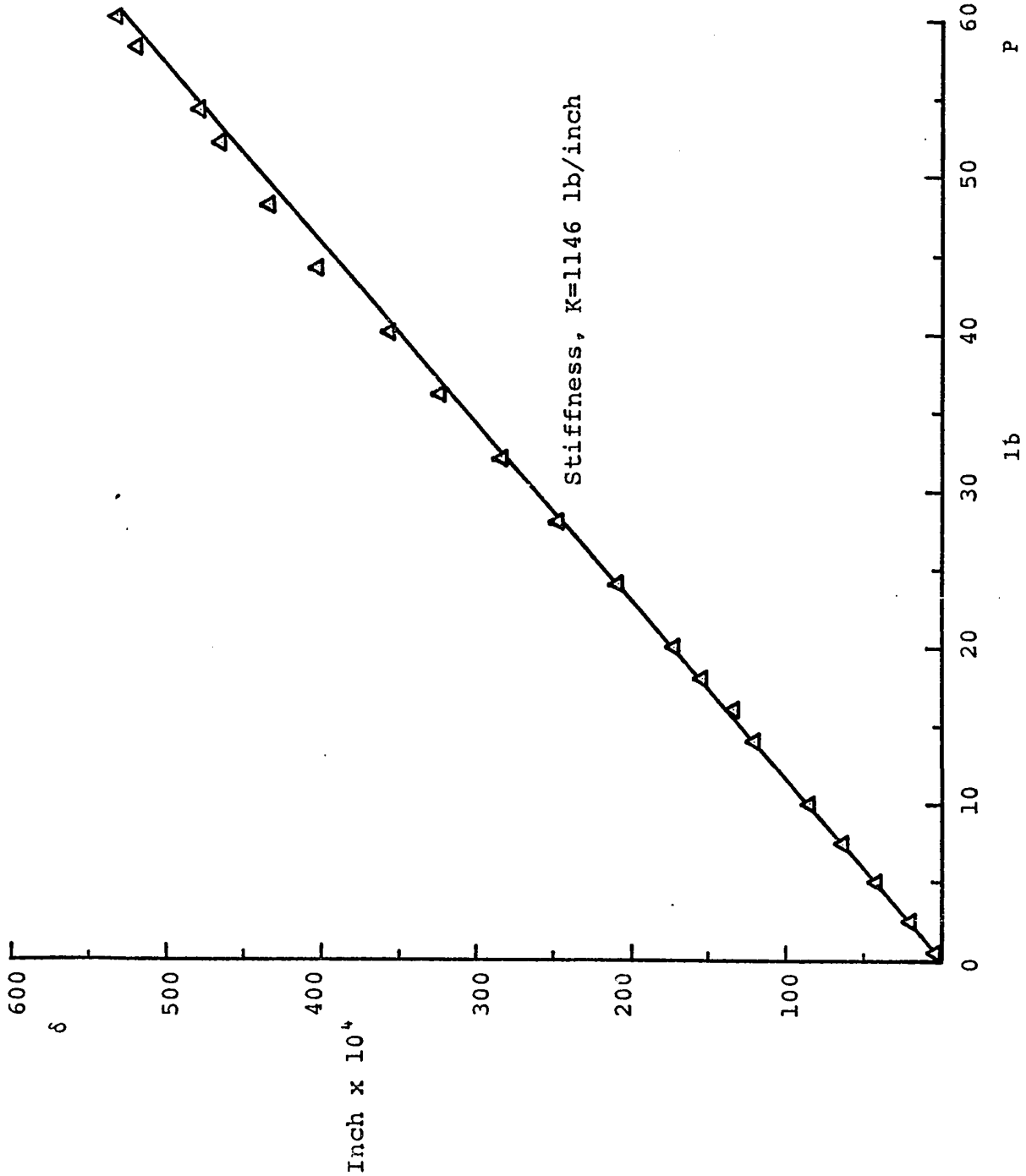

Fig.22 STIFFNESS OF THE FORCE GAUGE

Fig.23 STRIP CHART RECORDS

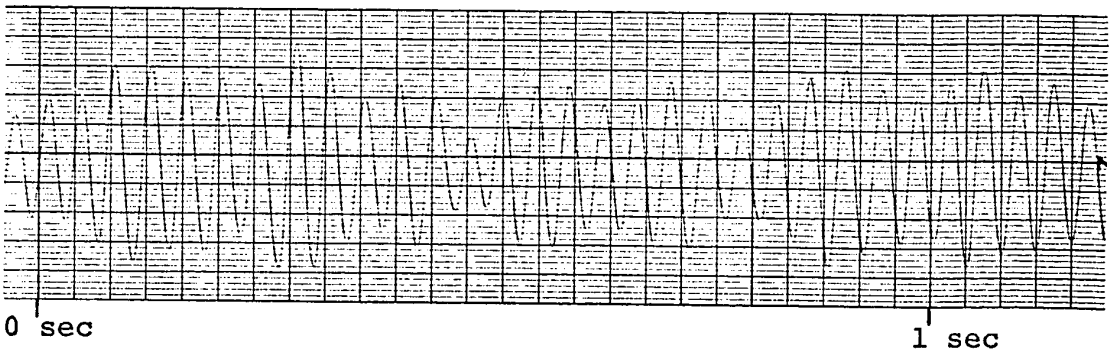

Circular Cylinder: Run No.1304000003
d=4", f=25.6 cps
Recorder Speed: 125 mm/sec.

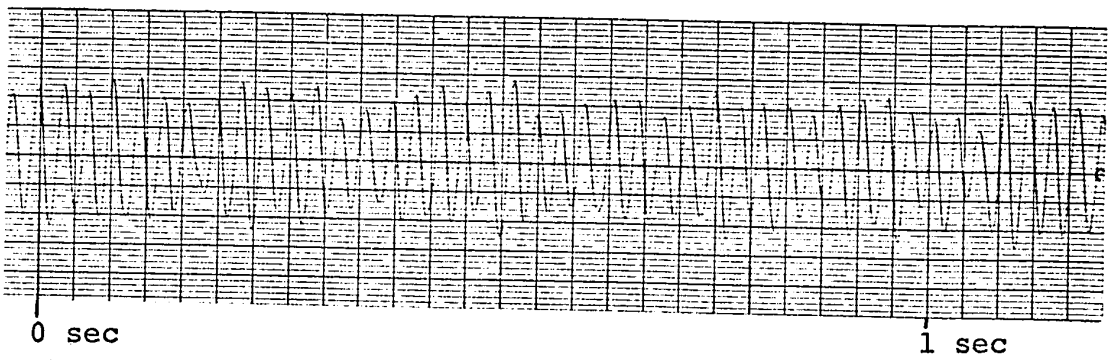

Triangle(prism): Run No.2306030005
b=6", θ=30°, f=36.35 cps
Recorder Speed: 125 mm/sec.

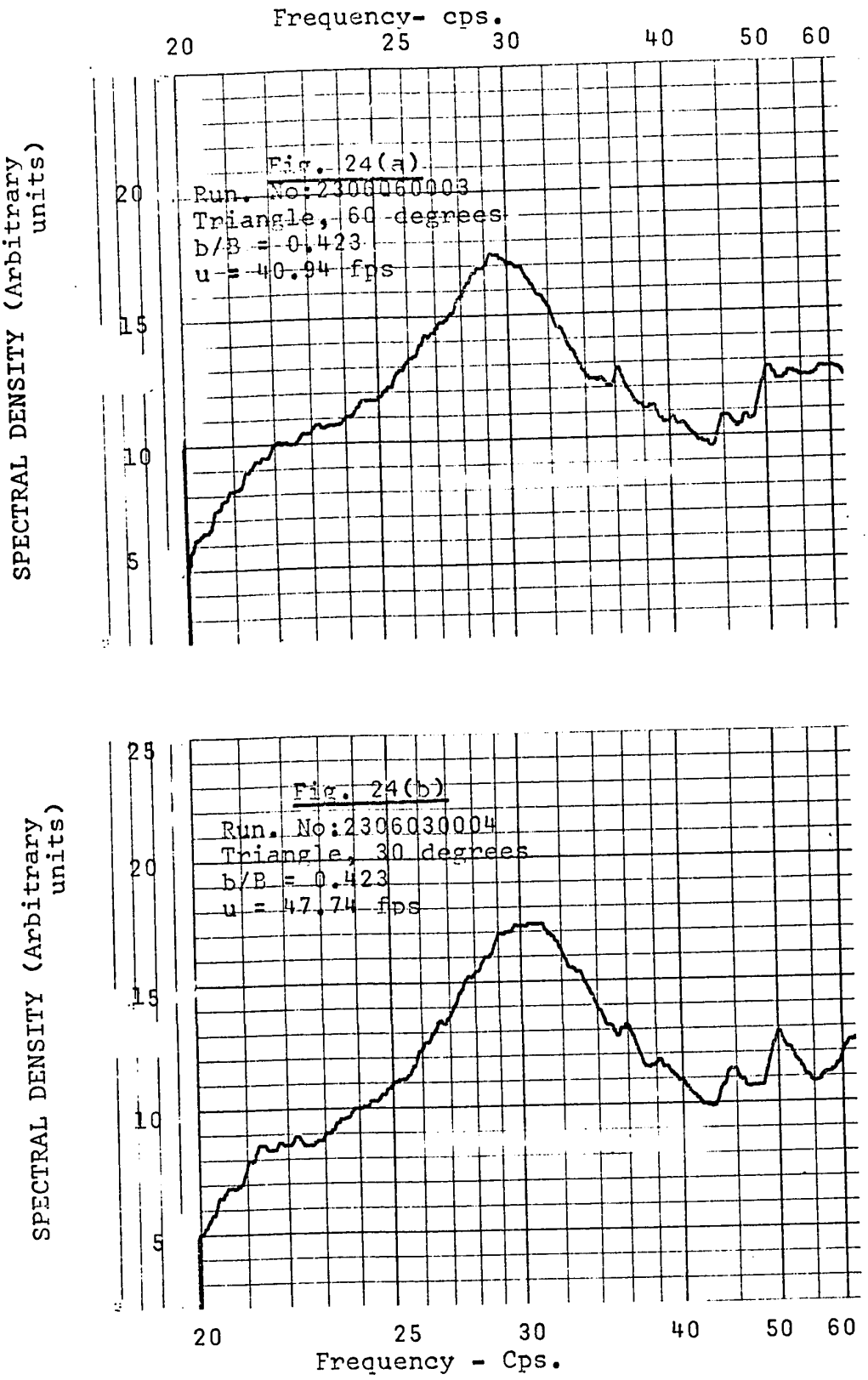

FIG. 24. SPECTRAL PLOTS

(a) Force Gage

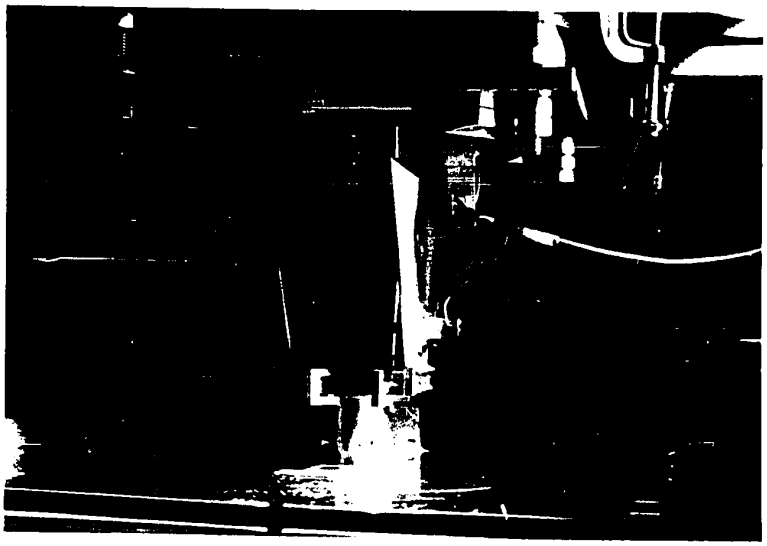

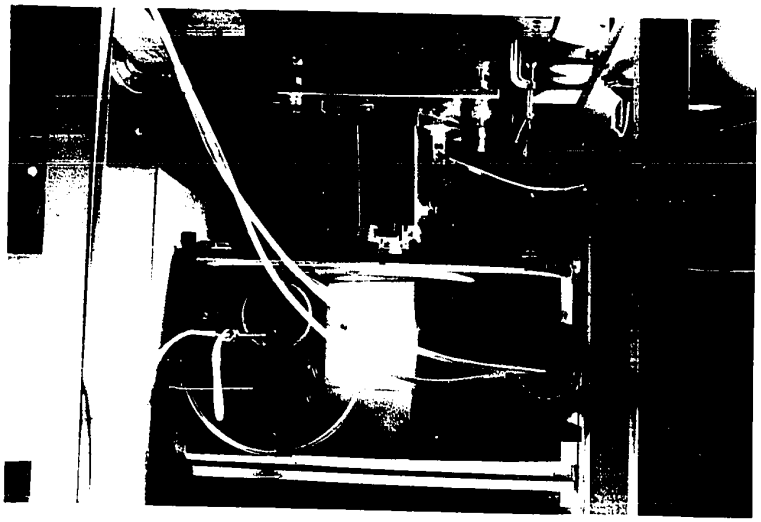

(b) Test Section

(c) Wind Tunnel & Auxiliary Equipment

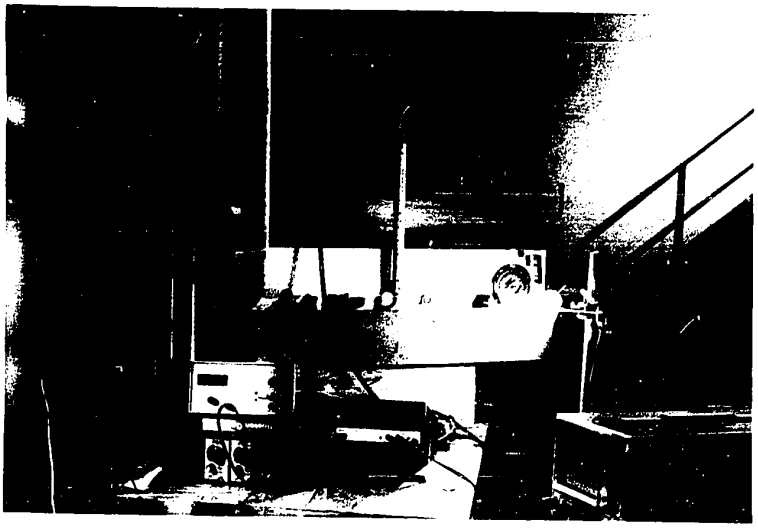

Fig.25 PHOTOGRAPH OF EQUIPMENT

(a) Force Gage

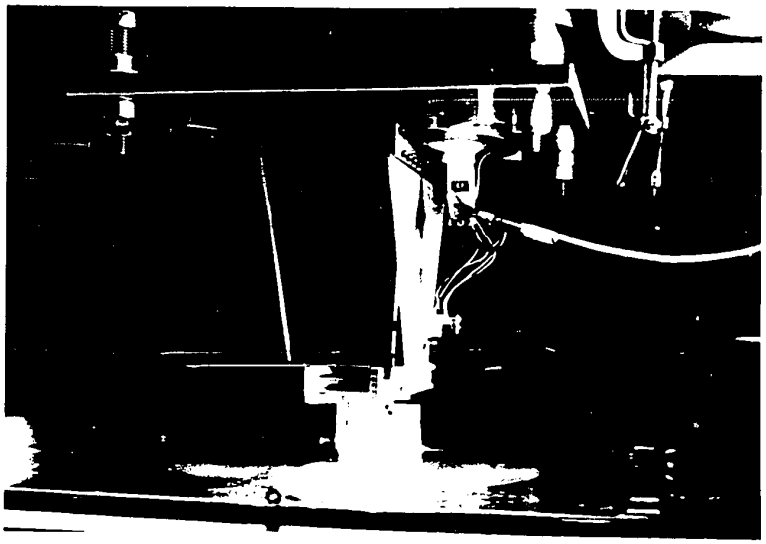

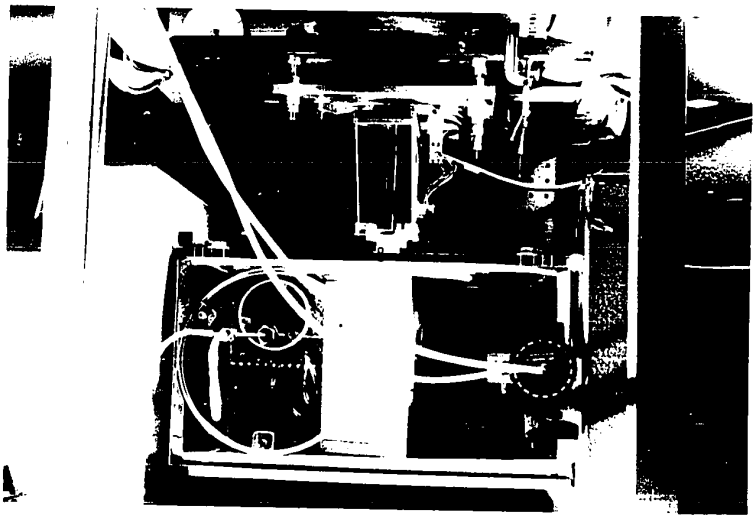

(b) Test Section

(c) Wind Tunnel & Auxiliary Equipment

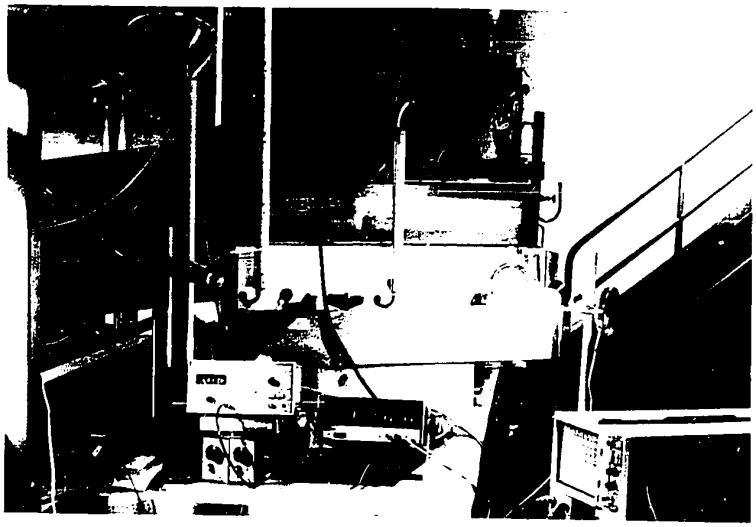

Fig.25 PHOTOGRAPH OF EQUIPMENT

FIG. 26 ECCENTRIC MOUNTING
PARTIAL ROW EQUIVALENCE

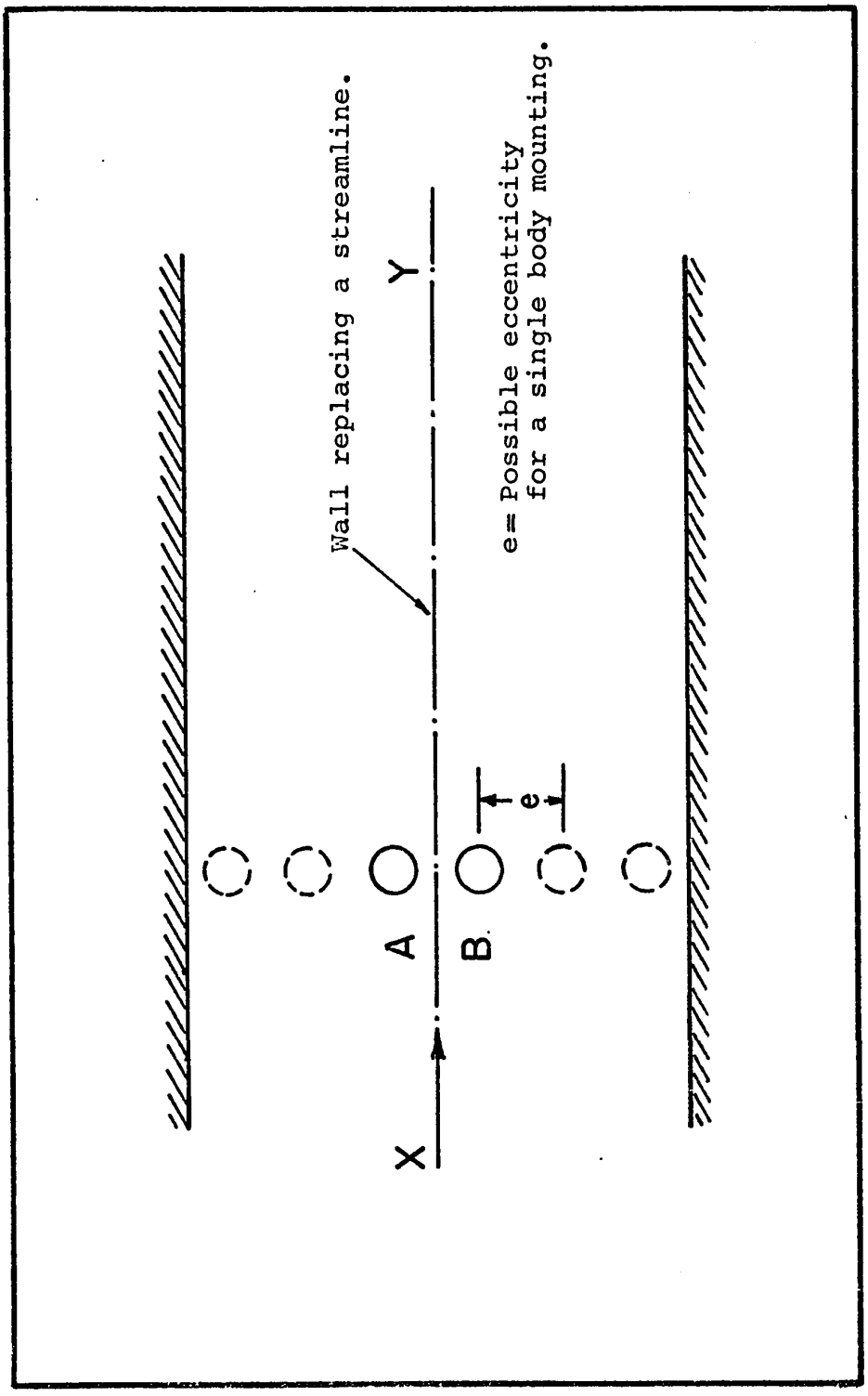

APPENDIX 4

EXISTING STROUHAL NUMBER PROPOSITIONS

The normal form of the Strouhal number $S = \frac{fd}{u}$ adopts the lateral dimension of the body d and the undisturbed velocity u as the length and velocity scales. The value of S varies widely for different bodies[28]. Fage[38] defined a Strouhal number based on the wake width b' (Fig.1) and the velocity u and obtained a nearly constant value ($\simeq$0.275) for a number of two dimensional bluff shapes.

Roshko[16] proposed the notched hodograph model and this yields the wake width b' for a given body shape and size. Roshko used this wake width and the wake velocity u_s to form the so called universal Strouhal number. This was shown to be a constant ($\simeq$0.16) in unconfined flows for all the bluff shapes tested by him.

Abernathy[17] extended Roshko's notched hodograph theory to flow past a flat plate set at varying inclinations in a confined flow. He was able to show that the experimental values of the Strouhal number ($\simeq$0.15) based on the wake width and the wake velocity was invariant for a large number of plate inclinations and flow confinements.

Tozkas[18] and Chen[19] used the contracted jet velocity u_j (Fig.1) and the wake width b' to form the Strouhal number for bluff shapes set in a confined flow. This Strouhal number

was found to be a constant ($\simeq 0.20$) for a limited range of blockages.

Bearman[39] proposed a universal Strouhal number, which used u_s as the velocity scale and the lateral distance between the vortex street h as the length scale. This Strouhal number had a constant value of about 0.18 for a variety of bluff shapes. Some of these shapes included wake interference elements. However, this Chen[40] states that Bearman's Strouhal number is invariant only in the subcritical Reynolds number range. Yet another dimensionless frequency number termed as the "wake number" was proposed by Chen[40]. It is based on some characteristics parameters of the vortex street. It is defined as $C = fh^2/\Gamma$, where f is the vortex shedding frequency, h is the lateral distance between the vorticies and Γ is the circulation associated with the vorticies. The wake number C is supposed to maintain a constant value of 0.165 over the entire range of Reynolds numbers spanning both subcritical and supercritical flows.

Vickery[41] has also tried to propose a correction for blocked flows. According to him, the increase in the value of the Strouhal number in confined flow is a result of the increase in the value of the separation velocities. Thus,

$$\frac{S}{S_c} = \frac{k_c}{k} \quad \ldots\ldots\ldots\ldots \quad (5\text{-}1)$$

where,

$k = \frac{u_s}{u}$

k_c = corrected value of k,

S = Strouhal number,

S_c = corrected value of S

Vickery's logic was developed on the basis of Maskell's theory which is limited to very low blockages. However, equation (5-1) seems to be logical from purely dimensional arguments, even for large blockages.

Toebes[12] proposed a strouhal number for blocked flows based on dimensional considerations. No attempt was made to provide a universal number. However, for confined flows where the contraction coefficient C_c varied with blockage, the contracted jet velocity u_j was shown to be the proper scaling factor. For situations where C_C was a weak function of blockage, the gap velocity u_1 was shown to be the proper scaling factor. The lateral body dimensions were used for the length scale. The present data reduction procedure has adopted this method and the test data has in general confirmed the earlier findings of Toebes[12]. It is concievable that one can obtain the wake characteristics such as the lateral distance "h" between the vorticies of the wake based on existing theoretical models[39]. When these are used in place of the body dimension, the contracted jet velocity may lead to strouhal numbers which are constant for all blockages and all shapes. A simple program (Tables 21 & 22) was developed to relate the vortex

street parameters with the body dimensions using existing approaches[39,40].

APPENDIX 5

Data Comparison

For comparison purposes the data from various sources are compiled and tabulated in Tables 1 to 6. Generally, the present data appears to compare favourably with data reported by other investigators, where overlaps are present. This is true for the data where the body shapes are comparable (Ex: flat plate and triangular prism with $\theta = 0^{\circ}$).

DATA COMPARISON

Table 1: Drag Coefficients C_D, C_{D1} - Cylinder

SHAPE	$\frac{b}{B}$ %	C_D	C_{D1}	SOURCE	R E M A R K S
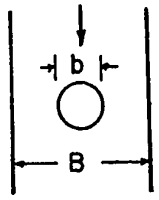	9.5	1.30	1.06	MODI[10]	Only averaged data in the sub-critical range (steady) is included.
	15.8	1.40	.99		
	22.0	1.50	.91		
	28.5	1.85	.95		
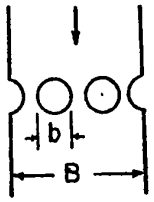	13.9	1.13	.84	NECE[33]	Open channel flow Multiple body configuration.
	27.9	1.57	.82		
	41.7	2.25	.76		
	55.6	4.25	.84		
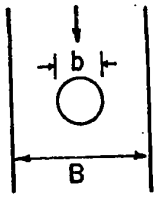	7.1	1.255	1.083	PRESENT DATA	Only averaged data in the sub-critical range (steady) is included.
	14.1	1.460	1.077		
	21.2	1.713	1.064		
	28.2	1.978	1.020		

Table 2: Drag Coefficients, C_D, C_{Dl} and C_{Dj} -

PLATE AND TRIANGLE(PRISM)

SHAPE	$\frac{b}{B}$ %	C_D	C_{Dl}	C_{Dj}	SOURCE	R E M A R K S
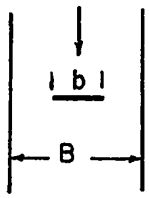	23.1	2.7	1.60	.83	SHAW[9]	C_{Dj} deviates from steady value when blockage is low.
	44.5	7.0	2.16	.95		
	66.7	22.0	2.44	.97		
	9.7	2.70	2.20	1.34	TOEBES[11,12]	Estimate from graph.
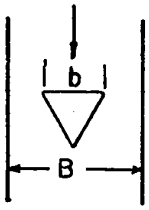	7.1	2.380	2.056	1.234	PRESENT DATA	
	14.1	2.834	2.091	1.176		
	21.2	3.628	2.256	1.169		
	28.2	4.342	2.239	1.114		
	42.3	7.502	2.498	1.104		
	56.4	14.463	2.751	1.125		
	70.5	34.433	3.000	1.171		

Table 3: Drag & Lift Coefficients C_D, C_{D1}, C_L and C_{L1}

- TRIANGLE(PRISM)

SHAPE	$\frac{b}{B}$ %	C_D	C_{D1}	C_L	C_{L1}	SOURCE	REMARKS
	9.7	1.94	1.581			TOEBES[11,12]	
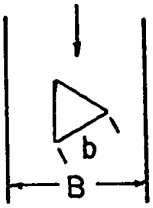	7.1	1.994	1.723			PRESENT DATA	
	14.1	2.139	1.578				
	21.2	2.424	1.507				
	28.2	2.612	1.347				
	42.3	4.058	1.352				
	56.4	6.901	1.313				
	70.5	11.801	1.028				
	9.7	1.40	1.141			TOEBES[11,12]	
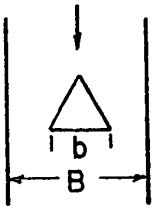	7.1	1.438	1.242			PRESENT DATA	
	14.1	1.590	1.173				
	21.2	1.977	1.229				
	28.2	2.292	1.182				
	42.3	3.702	1.233				
	56.4	6.460	1.229				
	70.5	15.800	1.376				
	9.7			1.31	1.067	TOEBES[11,12]	
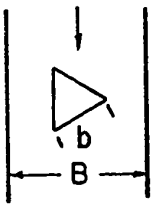	7.1			1.439	1.243	PRESENT DATA	
	14.1			1.578	1.165		
	21.2			1.852	1.152		
	28.2			2.303	1.187		
	42.3			3.438	1.145		
	56.4			6.534	1.277		
	70.5			13.028	1.135		

Table 4: Strouhal Number S and S_1 - CYLINDER

SHAPE	$\frac{b}{B}$ %	S	S_1	SOURCE	R E M A R K S
	6.0	.210	.197	TOEBES[11,12]	
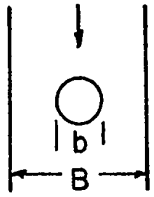	11.0	.215	.191		Estimate from graph.
	16.3	.235	.197		
	22.0	.245	.191		
	28.5	.255	.182		
	35.0	.278	.181		
	44.5	.330	.183		
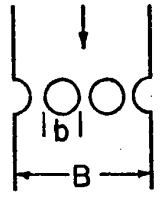	19.0		.16 & .19	BORGES[34]	Estimate from graph.
	25.0		.17 & .19		
	30.0		.17		
	38.0		.16 & .18		
	77.0		.18 & 7.3		
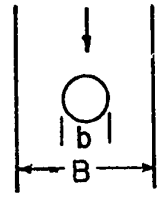	7.1	.205	.191	PRESENT DATA	
	14.1	.221	.190		
	21.2	.235	.185		
	28.2	.255	.183		
	42.3	.329	.190		

Table 5: Strouhal Number S and S_1 - TRIANGLE(PRISM)

SHAPE	$\frac{b}{B}$ %	S	S_1	SOURCE	R E M A R K S
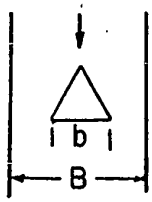	9.7	.237	.214	TOEBES[11,12]	Estimate from graph
	13.5	.237	.205		
	21.5	.256	.201		
	32.0	.285	.194		
	43.0	.345	.197		
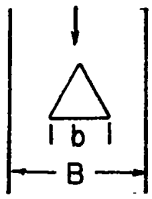	7.1	.233	.216	PRESENT DATA	
	14.1	.241	.207		
	21.2	.259	.204		
	28.2	.285	.205		
	42.3	.356	.205		
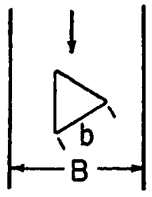	7.1	.180	.170	PRESENT DATA	
	14.1	.194	.167		
	21.2	.205	.161		
	28.2	.230	.165		
	42.3	.310	.179		

Table 6: Strouhal Number S, S_1 and S_j -

PLATE, GATE & TRIANGLE(PRISM)

SHAPE	$\frac{b}{B}$%	S	S_1	S_j	SOURCE	R E M A R K S
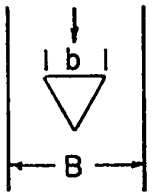	9.7	.155	.140	.109	TOEBES[11,12]	Estimate from graph
	13.5	.167	.144	.109		
	21.5	.190	.149	.108		
	32.0	.243	.165	.114		
	43.0	.365	.208	.138		
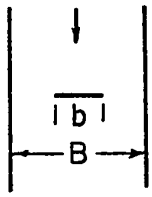	5.6	.154	.145	.145*	SHAW[9] "PLATE"	Estimate from graph.
	11.1	.176	.156	.120		
	16.7	.197	.164	.121		
	22.2	.210	.163	.118		
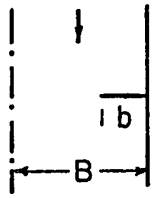	5.6	.160	.151	.151*	SHAW[9] "GATE"	Estimate from graph
	11.1	.188	.167	.129		
	16.7	.205	.171	.126		
	22.2	.216	.168	.121		
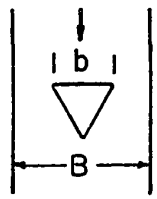	7.1	.148	.137	.109		
	14.1	.166	.143	.107	PRESENT DATA	
	21.2	.185	.146	.105		
	28.2	.223	.160	.112		
	42.3	.371	.214	.142		

*Blockage far too low - Procedure for data reduction not applicable.

APPENDIX 6

APPENDIX 6

VELOCITY DISTRIBUTION

The velocity distribution at the test-section was reasonably uniform (Fig.20). In the range of test section velocity (u) used, the velocity distribution did not appear to change very much. For clarity, the distribution for only one velocity is shown.

TRANSDUCER CALIBRATION

The force gauge had a large range of deflections in which it was linear with respect to loading. However, the LVDT (Linear Voltage Differential Transformer) transducer had a limited range of linearity with respect to loading (Fig.21). This linear range is denoted by the limits of the line AA' in Fig.21.

FORCE GAUGE COMPUTATION

The experimental stiffness coefficient $K=\frac{P}{\delta}$ denoting the load (lb) per unit deflection (in.) was obtained by direct calibration (Fig.22). The resulting value of K was 1146 lb/in.

For the effective mass[35] of the gauge "m" from the point of view of vibration, the mass of the lower bridging bracket, the lower collar plates, the fastening screws and the lower third of the side plates were included, in gauge frequency

computation. The computation gave the value of .001676 lb·sec^2/inch for the effective gauge mass. The frequency "f" of the gauge was estimated as follows:

$$f = \frac{1}{2\pi}\sqrt{\frac{K}{m}} = \frac{1}{2\pi}\sqrt{\frac{1146}{.001676}} = 131 \text{ cps}$$

The experiment value of the frequency and the damping coefficient are given below:

f = 129.5 cps

β = 0.042 lb.sec/inch

ζ = 0.015 (logarithmic decrement) = $\frac{\beta}{\beta_c}$

APPENDIX 7.

COMPUTER PROGRAMS AND OUTPUTS

A simple computer program was developed to facilitate data reduction. One version of the program and reduced data are shown in tables 7 to 22.

```
PROGRAM     DRAG                                CDC 6600 FTN V3.0-P296 OPT=1  72/08/05. 15.32.32.

            PROGRAM DRAG (INPUT,OUTPUT,TAPE60=INPUT)
      C     TO FIND CD,FLOW PROP.--68 DEG F.
            INTEGER RUNNO,RUN1,RUN2,RUN3,RUN4
          5 FORMAT(1H1,/////6X,5HRUNNO,5X,3HDIA,4X,6HDELTAH,6X,4HVOLT,
     5      15X,4HGAIN,3X,8HVELOCITY, 9X,5HREYNO,5X,5HFORCE,8X,2HCD,8X,2HCL,
           27X,3HCDI)
         10 FORMAT(I10,F5.1,2F10.3,F10.1)
         20 FORMAT(1X,I10,F8.1,2F10.3, F9.1,F11.2,E14.4,2F10.3,F20.3)
         30 FORMAT(/)
         40 FORMAT(1X,I10,F8.1,2F10.3, F9.1,F11.2,E14.4,F10.3,F20.3,F10.3)
    10     RNU=0.00016
           GAMMA=0.07535
           DENSITY=0.00234
           B=14.1875
           CC=1.0
    15     PRINT 5
           DIA2=1.0
           RUN2=0
         50 READ (60,10)RUNNO,DIA,DELTAH,VOLT,GAIN
           IF(EOF(60))110,60
    20   60 V=18.29*(SQRT(DELTAH/GAMMA))*0.975
      C     CORRECTION FACTOR .975 IS TAKEN AS FROM THE FACT THAT MEAN VEL.
      C     IS LOWER THAN THE MAX.VEL. AND THE TEST SECTION IS DIVERGENT.
           REYNO=(V*DIA)/(12.*RNU)
    25     RUN4=RUNNO/10000000
           IF(RUN4 .EQ. 111)GO TO 65
           IF(RUNNO .LT. 2000000000 .AND. RUN4 .NE. 111)GO TO 70
           IF(RUNNO .GT. 2104000000 .AND. RUNNO .LT. 2106080000)GO TO 70
           IF(RUNNO .GT. 2204030000 .AND. RUNNO .LT. 2206070000)GO TO 70
    30     FORCE=VOLT/(.1471*GAIN)
           GO TO 75
         65 FORCE=VOLT/(.0986*GAIN)
           GO TO 75
         70 FORCE=VOLT/(.1012*GAIN)
    35   75 AREA=(9.75*DIA)/144.
           CD=(2.*FORCE)/(DENSITY*V*V*AREA)
           CDJ=CD*(CC*(B-DIA)/B)*(CC*(B-DIA)/B)
           DIA1=DIA
           IF(DIA1 .NE. DIA2)GO TO 85
    40   83 RUN1=RUNNO/1000
           IF(RUN1 .NE. RUN2/1000)GO TO 90
           GO TO 95
         85 PRINT 5
           GO TO 83
    45   90 PRINT 30
         95 RUN3=RUNNO/100000000
           IF(RUN3 .EQ.22)GO TO 100
           PRINT 20,RUNNO,DIA,DELTAH,VOLT,GAIN,V,REYNO,FORCE,CD,CDJ
           GO TO 105
    50   100 PRINT 40,RUNNO,DIA,DELTAH,VOLT,GAIN,V,REYNO,FORCE,CD,CDJ
        105 RUN2=RUNNO
           DIA2=DIA
           GO TO 50
        110 STOP
    55     END
```

Table 7: Steady Force Coefficients program.

Table 8: Drag and Lift Coefficients - reduced data, 1" body, b/B = 0.071

RUNNO	DIA	DELTAH	VOLT	GAIN	VELOCITY	REYNO	FORCE	CD	CL	CD1	SHAPE
											Circle Drag
1101000001	1.0	.140	.064	10.0	24.31	.1266E+05	.063	1.351		1.167	
1101000002	1.0	.330	.149	10.0	37.32	.1944E+05	.147	1.334		1.153	
1101000003	1.0	.760	.324	10.0	56.63	.2950E+05	.320	1.260		1.089	
1101000004	1.0	1.360	.571	10.0	75.76	.3946E+05	.564	1.241		1.072	
1101000005	1.0	2.170	.890	10.0	95.70	.4984E+05	.879	1.212		1.047	
1101000006	1.0	3.032	1.256	10.0	113.12	.5892E+05	1.241	1.224		1.058	
1101000007	1.0	4.150	1.702	10.0	132.34	.6893E+05	1.682	1.212		1.047	
1101000008	1.0	5.410	2.201	10.0	151.10	.7870E+05	2.175	1.202		1.039	
											Triangle θ=0° Drag
2101000001	1.0	.141	.163	10.0	24.39	.1271E+05	.111	2.351		2.031	
2101000002	1.0	.330	.384	10.0	37.32	.1944E+05	.261	2.366		2.044	
2101000003	1.0	.758	.892	10.0	56.56	.2946E+05	.606	2.393		2.067	
2101000004	1.0	1.333	1.569	10.0	75.01	.3907E+05	1.067	2.393		2.068	
2101000005	1.0	2.121	2.501	10.0	94.61	.4928E+05	1.700	2.398		2.072	
2101000006	1.0	3.025	3.571	10.0	112.99	.5885E+05	2.428	2.400		2.074	
2101000007	1.0	4.165	4.866	10.0	132.58	.6905E+05	3.308	2.376		2.052	
2101000008	1.0	5.440	6.320	10.0	151.52	.7892E+05	4.296	2.362		2.041	
											Triangle θ=30° Drag
2101030001	1.0	.141	.128	10.0	24.39	.1271E+05	.087	1.846		1.595	
2101030002	1.0	.329	.322	10.0	37.26	.1941E+05	.219	1.990		1.719	
2101030003	1.0	.751	.744	10.0	56.30	.2932E+05	.506	2.014		1.740	
2101030004	1.0	1.338	1.331	10.0	75.15	.3914E+05	.905	2.023		1.748	
2101030005	1.0	2.130	2.120	10.0	94.81	.4938E+05	1.441	2.024		1.749	
2101030006	1.0	3.035	3.018	10.0	113.18	.5895E+05	2.052	2.022		1.747	
2101030007	1.0	4.160	4.130	10.0	132.50	.6901E+05	2.808	2.019		1.744	
2101030008	1.0	5.420	5.377	10.0	151.24	.7877E+05	3.655	2.017		1.743	
											Triangle θ=60° Drag
2101060001	1.0	.142	.114	10.0	24.48	.1275E+05	.077	1.632		1.410	
2101060002	1.0	.328	.248	10.0	37.21	.1938E+05	.169	1.537		1.328	
2101060003	1.0	.754	.543	10.0	56.41	.2938E+05	.369	1.464		1.265	
2101060004	1.0	1.350	.933	10.0	75.48	.3931E+05	.634	1.405		1.214	
2101060005	1.0	2.112	1.439	10.0	94.41	.4917E+05	.978	1.385		1.197	
2101060006	1.0	3.042	2.044	10.0	113.31	.5901E+05	1.390	1.366		1.180	
2101060007	1.0	4.157	2.790	10.0	132.45	.6899E+05	1.897	1.365		1.179	
2101060008	1.0	5.410	3.578	10.0	151.10	.7870E+05	2.432	1.345		1.162	
											Triangle θ=30° Lift
2201030001	1.0	.141	.104	10.0	24.39	.1271E+05	.071		1.500	1.296	
2201030002	1.0	.330	.237	10.0	37.32	.1944E+05	.161		1.460	1.262	
2201030003	1.0	.758	.538	10.0	56.56	.2946E+05	.366		1.443	1.247	
2201030004	1.0	1.340	.944	10.0	75.20	.3917E+05	.642		1.432	1.238	
2201030005	1.0	2.118	1.481	10.0	94.55	.4924E+05	1.007		1.422	1.228	
2201030006	1.0	3.040	2.116	10.0	113.27	.5899E+05	1.438		1.415	1.223	
2201030007	1.0	4.155	2.899	10.0	132.42	.6897E+05	1.971		1.419	1.226	
2201030008	1.0	5.410	3.777	10.0	151.10	.7870E+05	2.568		1.420	1.227	

Table 9: Drag and Lift Coefficients - reduced data, 2" body, b/B= 0.141

RUNNO	DIA	DELTAH	VOLT	GAIN	VELOCITY	REYNO	FORCE	CD	CL	CD1	SHAPE
											Circle Drag
1102000001	2.0	.519	.537	10.0	46.80	.4875E+05	.531	1.529		1.128	
1102000002	2.0	.732	.749	10.0	55.58	.5790E+05	.740	1.512		1.116	
1102000003	2.0	1.042	1.022	10.0	66.31	.6908E+05	1.010	1.449		1.070	
1102000004	2.0	1.385	1.365	10.0	76.45	.7964E+05	1.349	1.456		1.075	
1102000005	2.0	2.486	2.420	10.0	102.43	.1067E+06	2.391	1.439		1.062	
1102000006	2.0	3.515	3.271	10.0	121.80	.1269E+06	3.232	1.375		1.015	
											Triangle θ=0° Drag
2102000001	2.0	.525	.143	1.0	47.07	.4903E+05	.972	2.769		2.043	
2102000002	2.0	.730	.199	1.0	55.51	.5782E+05	1.353	2.771		2.045	
2102000003	2.0	1.039	.288	1.0	66.22	.6898E+05	1.958	2.818		2.080	
2102000004	2.0	1.370	.382	1.0	76.04	.7921E+05	2.597	2.835		2.092	
2102000005	2.0	2.485	.712	1.0	102.41	.1067E+06	4.840	2.913		2.150	
2102000006	2.0	3.520	1.003	1.0	121.88	.1270E+06	6.818	2.897		2.138	
											Triangle θ=30° Drag
2102030001	2.0	.530	.111	1.0	47.29	.4927E+05	.755	2.129		1.571	
2102030002	2.0	.734	.155	1.0	55.66	.5798E+05	1.054	2.147		1.584	
2102030003	2.0	1.047	.220	1.0	66.47	.6924E+05	1.496	2.136		1.576	
2102030004	2.0	1.375	.290	1.0	76.18	.7935E+05	1.971	2.144		1.582	
2102030005	2.0	2.492	.529	1.0	102.55	.1068E+06	3.596	2.158		1.593	
2102030006	2.0	3.520	.733	1.0	121.88	.1270E+06	4.983	2.117		1.562	
											Triangle θ=60° Drag
2102060001	2.0	.516	.082	1.0	46.67	.4861E+05	.557	1.616		1.192	
2102060002	2.0	.738	.116	1.0	55.81	.5813E+05	.789	1.598		1.179	
2102060003	2.0	1.045	.162	1.0	66.41	.6918E+05	1.101	1.576		1.163	
2102060004	2.0	1.385	.211	1.0	76.45	.7964E+05	1.434	1.549		1.143	
2102060005	2.0	2.484	.397	1.0	102.39	.1067E+06	2.699	1.625		1.199	
2102060006	2.0	3.520	.546	1.0	121.88	.1270E+06	3.712	1.577		1.164	
											Triangle θ=30° Lift
2202030001	2.0	.515	.799	10.0	46.62	.4856E+05	.543		1.577	1.164	
2202030002	2.0	.728	1.135	10.0	55.43	.5774E+05	.772		1.585	1.170	
2202030003	2.0	1.047	.160	1.0	66.47	.6924E+05	1.088		1.554	1.146	
2202030004	2.0	1.371	.214	1.0	76.07	.7924E+05	1.455		1.587	1.171	
2202030005	2.0	2.484	.385	1.0	102.39	.1067E+06	2.617		1.576	1.163	
2202030006	2.0	3.510	.549	1.0	121.71	.1268E+06	3.732		1.590	1.173	

Table 10: Drag and Lift Coefficients - reduced data, 3" body, b/B = 0.212

RUNNO	DIA	DELTAH	VOLT	GAIN	VELOCITY	REYNO	FORCE	CD	CL	CD1	SHAPE
1103000001	3.0	.228	.408	10.0	31.02	.4847E+05	.403	1.763		1.096	Circle Drag
1103000002	3.0	.330	.577	10.0	37.32	.5831E+05	.570	1.723		1.071	
1103000003	3.0	.450	.778	10.0	43.58	.6809E+05	.769	1.703		1.059	
1103000004	3.0	.605	1.021	10.0	50.53	.7895E+05	1.009	1.663		1.034	
1103000005	3.0	1.105	1.778	10.0	68.29	.1067E+06	1.757	1.585		.986	
1103000006	3.0	1.530	2.364	10.0	80.36	.1256E+06	2.336	1.522		.947	
1103000007	3.0	2.135	3.118	10.0	94.92	.1483E+06	3.081	1.439		.895	
2103000010	3.0	.230	.122	1.0	31.16	.4868E+05	.829	3.595		2.235	Triangle θ= 0° Drag
2103000011	3.0	.329	.175	1.0	37.26	.5822E+05	1.190	3.605		2.242	
2103000012	3.0	.457	.241	1.0	43.92	.6862E+05	1.638	3.574		2.222	
2103000013	3.0	.610	.339	1.0	50.74	.7928E+05	2.305	3.767		2.342	
2103000014	3.0	1.108	.588	1.0	68.38	.1068E+06	3.997	3.597		2.237	
2103000015	3.0	1.558	.834	1.0	81.09	.1267E+06	5.670	3.628		2.256	
2103030001	3.0	.230	.083	1.0	31.16	.4868E+05	.564	2.446		1.521	Triangle θ=30° Drag
2103030002	3.0	.326	.117	1.0	37.09	.5796E+05	.795	2.433		1.513	
2103030003	3.0	.461	.167	1.0	44.11	.6892E+05	1.135	2.455		1.527	
2103030004	3.0	.608	.218	1.0	50.66	.7915E+05	1.482	2.430		1.511	
2103030005	3.0	1.115	.398	1.0	68.60	.1072E+06	2.706	2.419		1.504	
2103030006	3.0	1.558	.551	1.0	81.09	.1267E+06	3.746	2.397		1.490	
2103030007	3.0	2.100	.739	1.0	94.14	.1471E+06	5.024	2.385		1.483	
2103060001	3.0	.231	.069	1.0	31.22	.4879E+05	.469	2.025		1.259	Triangle θ=60° Drag
2103060002	3.0	.328	.096	1.0	37.21	.5813E+05	.653	1.984		1.233	
2103060003	3.0	.460	.136	1.0	44.06	.6885E+05	.925	2.004		1.246	
2103060004	3.0	.615	.179	1.0	50.95	.7960E+05	1.217	1.973		1.227	
2103060005	3.0	1.108	.316	1.0	68.38	.1068E+06	2.148	1.933		1.202	
2103060006	3.0	1.542	.455	1.0	80.67	.1260E+06	3.093	2.000		1.244	
2103060007	3.0	2.120	.601	1.0	94.59	.1478E+06	4.086	1.921		1.195	
2203030001	3.0	.228	.064	1.0	31.02	.4847E+05	.435		1.903	1.183	Triangle θ=30° Lift
2203030002	3.0	.329	.089	1.0	37.26	.5822E+05	.605		1.833	1.140	
2203030003	3.0	.461	.126	1.0	44.11	.6892E+05	.857		1.852	1.152	
2203030004	3.0	.608	.164	1.0	50.66	.7915E+05	1.115		1.828	1.137	
2203030005	3.0	1.111	.312	1.0	68.48	.1070E+06	2.121		1.903	1.184	
2203030006	3.0	1.555	.417	1.0	81.01	.1266E+06	2.835		1.818	1.130	
2203030007	3.0	2.125	.564	1.0	94.70	.1480E+06	3.834		1.799	1.119	
2203030008	3.0	.231	.064	1.0	31.22	.4879E+05	.435		1.878	1.168	

Table 11: Drag and Lift Coefficients - reduced data, 4" body, b/B = 0.282

RUNNO	DIA	DELTAH	VOLT	GAIN	VELOCITY	REYNO	FORCE	CD	CL	CD1	SHAPE
											Circle Drag
1104000001	4.0	.125	.340	10.0	22.97	.4785E+05	.336	2.010		1.036	
1104000002	4.0	.183	.496	10.0	27.79	.5790E+05	.490	2.003		1.033	
1104000003	4.0	.261	.691	10.0	33.19	.6914E+05	.683	1.956		1.009	
1104000004	4.0	.334	.878	10.0	37.54	.7822E+05	.868	1.942		1.001	
1104000005	4.0	.660	1.660	10.0	52.78	.1100E+06	1.640	1.858		.958	
1104000006	4.0	.890	2.139	10.0	61.29	.1277E+06	2.114	1.776		.916	
1104000007	4.0	1.202	2.745	10.0	71.22	.1484E+06	2.712	1.687		.870	
											Triangle θ=0° Drag
2104000001	4.0	.130	.078	1.0	23.42	.4880E+05	.771	4.433		2.286	
2104000002	4.0	.185	.107	1.0	27.94	.5821E+05	1.057	4.274		2.204	
2104000003	4.0	.265	.156	1.0	33.44	.6967E+05	1.542	4.350		2.243	
2104000004	4.0	.325	.189	1.0	37.04	.7716E+05	1.868	4.297		2.216	
2104000005	4.0	.652	.382	1.0	52.46	.1093E+06	3.775	4.329		2.232	
2104000006	4.0	.905	.535	1.0	61.80	.1288E+06	5.287	4.368		2.252	
2104000007	4.0	1.201	.706	1.0	71.19	.1483E+06	6.976	4.343		2.240	
											Triangle θ=30° Drag
2104030001	4.0	.145	.494	10.0	24.74	.5154E+05	.488	2.517		1.298	
2104030002	4.0	.178	.619	10.0	27.41	.5710E+05	.612	2.570		1.325	
2104030003	4.0	.255	.915	10.0	32.81	.6834E+05	.904	2.651		1.367	
2104030004	4.0	.320	.105	1.0	36.75	.7656E+05	1.038	2.424		1.250	
2104030005	4.0	.650	.238	1.0	52.38	.1091E+06	2.352	2.705		1.395	
2104030006	4.0	.888	.322	1.0	61.22	.1275E+06	3.182	2.679		1.381	
2104030007	4.0	1.205	.446	1.0	71.31	.1486E+06	4.407	2.735		1.410	
											Triangle θ=60° Drag
2104060001	4.0	.145	.045	1.0	24.74	.5154E+05	.445	2.293		1.182	
2104060002	4.0	.190	.060	1.0	28.32	.5899E+05	.593	2.333		1.203	
2104060003	4.0	.268	.084	1.0	33.63	.7007E+05	.830	2.316		1.194	
2104060004	4.0	.328	.101	1.0	37.21	.7751E+05	.998	2.275		1.173	
2104060005	4.0	.657	.207	1.0	52.66	.1097E+06	2.045	2.328		1.200	
2104060006	4.0	.890	.273	1.0	61.29	.1277E+06	2.698	2.266		1.169	
2104060007	4.0	1.200	.363	1.0	71.17	.1483E+06	3.587	2.235		1.152	
											Triangle θ=30° Lift
2204030001	4.0	.135	.043	1.0	23.87	.4973E+05	.425		2.353	1.213	
2204030002	4.0	.190	.059	1.0	28.32	.5899E+05	.583		2.294	1.183	
2204030003	4.0	.260	.080	1.0	33.13	.6901E+05	.791		2.273	1.172	
2204030004	4.0	.327	.101	1.0	37.15	.7739E+05	.998		2.282	1.177	
2204030005	4.0	.658	.207	1.0	52.70	.1098E+06	2.045		2.324	1.199	
2204030006	4.0	.888	.275	1.0	61.22	.1275E+06	2.717		2.288	1.180	
2204030007	4.0	1.200	.374	1.0	71.17	.1483E+06	3.696		2.303	1.187	

Table 12: Drag and Lift Coefficients - reduced data, 6" body, b/B = 0.423

RUNNO	DIA	DELTAH	VOLT	GAIN	VELOCITY	REYNO	FORCE	CD	CL	CD1	SHAPE
											Circle Drag
1106000001	6.0	.153	.099	1.0	25.41	.7941E+05	.978	3.187		1.062	
1106000002	6.0	.298	.150	1.0	35.46	.1108E+06	1.482	2.479		.826	
1106000003	6.0	.390	.195	1.0	40.57	.1268E+06	1.927	2.463		.820	
1106000004	6.0	.551	.260	1.0	48.22	.1507E+06	2.569	2.324		.774	
1106000005	6.0	.788	.288	1.0	57.67	.1802E+06	2.846	1.800		.600	
1106000006	6.0	1.310	.383	1.0	74.36	.2324E+06	3.785	1.440		.480	
											Triangle θ=0° Drag
2106000001	6.0	.153	.230	1.0	25.41	.7941E+05	2.273	7.405		2.466	
2106000002	6.0	.292	.442	1.0	35.10	.1097E+06	4.368	7.456		2.483	
2106000003	6.0	.400	.613	1.0	41.09	.1284E+06	6.057	7.549		2.514	
2106000004	6.0	.541	.830	1.0	47.78	.1493E+06	8.202	7.557		2.517	
2106000005	6.0	.780	1.191	1.0	57.38	.1793E+06	11.769	7.521		2.505	
2106000006	6.0	1.300	1.985	1.0	74.07	.2315E+06	19.615	7.521		2.505	
											Triangle θ=30° Drag
2106030001	6.0	.153	.128	1.0	25.41	.7941E+05	1.265	4.121		1.372	
2106030002	6.0	.300	.249	1.0	35.58	.1112E+06	2.460	4.089		1.362	
2106030003	6.0	.400	.326	1.0	41.09	.1284E+06	3.221	4.015		1.337	
2106030004	6.0	.540	.439	1.0	47.74	.1492E+06	4.338	4.005		1.334	
2106030005	6.0	.790	.649	1.0	57.74	.1804E+06	6.413	4.047		1.348	
2106030006	6.0	1.300	1.075	1.0	74.07	.2315E+06	10.623	4.073		1.357	
											Triangle θ=60° Drag
2106060001	6.0	.150	.112	1.0	25.16	.7863E+05	1.107	3.678		1.225	
2106060002	6.0	.305	.231	1.0	35.88	.1121E+06	2.283	3.731		1.242	
2106060003	6.0	.395	.296	1.0	40.83	.1276E+06	2.925	3.691		1.229	
2106060004	6.0	.538	.400	1.0	47.65	.1489E+06	3.953	3.662		1.220	
2106060005	6.0	.780	.594	1.0	57.38	.1793E+06	5.870	3.751		1.249	
2106060006	6.0	1.300	.976	1.0	74.07	.2315E+06	9.644	3.698		1.232	
											Triangle θ=30° Lift
2206030001	6.0	.150	.105	1.0	25.16	.7863E+05	1.038		3.448	1.148	
2206030002	6.0	.300	.212	1.0	35.58	.1112E+06	2.095		3.481	1.159	
2206030003	6.0	.400	.286	1.0	41.09	.1284E+06	2.826		3.522	1.173	
2206030004	6.0	.540	.374	1.0	47.74	.1492E+06	3.696		3.412	1.136	
2206030005	6.0	.810	.573	1.0	58.47	.1827E+06	5.662		3.485	1.161	
2206030006	6.0	1.315	.876	1.0	74.50	.2328E+06	8.656		3.281	1.093	

Table 13: Drag and Lift Coefficients - reduced data, 8" body, b/B = 0.564

RUNNO	DIA	DELTAH	VOLT	GAIN	VELOCITY	REYNO	FORCE	CD	CL	CDl	SHAPE
											Circle Drag
1108000001	8.0	.168	.220	1.0	26.63	.1109E+06	2.174	4.838		.920	
1108000002	8.0	.233	.273	1.0	31.36	.1307E+06	2.698	4.329		.823	
1108000003	8.0	.310	.285	1.0	36.17	.1507E+06	2.816	3.396		.646	
1108000004	8.0	.437	.344	1.0	42.95	.1789E+06	3.399	2.908		.553	
1108000005	8.0	.707	.542	1.0	54.62	.2276E+06	5.356	2.832		.539	
											Triangle θ=0° Drag
2108000001	8.0	.167	.952	1.0	26.55	.1106E+06	6.472	14.489		2.756	
2108000002	8.0	.232	1.312	1.0	31.29	.1304E+06	8.919	14.373		2.734	
2108000003	8.0	.320	1.835	1.0	36.75	.1531E+06	12.475	14.575		2.772	
2108000004	8.0	.445	2.537	1.0	43.34	.1806E+06	17.247	14.490		2.756	
2108000005	8.0	.705	3.991	1.0	54.55	.2273E+06	27.131	14.388		2.737	
											Triangle θ=30° Drag
2108030001	8.0	.168	.456	1.0	26.63	.1109E+06	3.100	6.899		1.312	
2108030002	8.0	.231	.624	1.0	31.22	.1301E+06	4.242	6.866		1.306	
2108030003	8.0	.304	.826	1.0	35.82	.1492E+06	5.615	6.906		1.314	
2108030004	8.0	.440	1.184	1.0	43.09	.1796E+06	8.049	6.839		1.301	
2108030005	8.0	.700	1.926	1.0	54.35	.2265E+06	13.093	6.993		1.330	
											Triangle θ=60° Drag
2108060001	8.0	.168	.418	1.0	26.63	.1109E+06	2.842	6.324		1.203	
2108060002	8.0	.230	.587	1.0	31.16	.1298E+06	3.990	6.487		1.234	
2108060003	8.0	.310	.787	1.0	36.17	.1507E+06	5.350	6.453		1.227	
2108060004	8.0	.440	1.117	1.0	43.09	.1796E+06	7.593	6.452		1.227	
2108060005	8.0	.718	1.860	1.0	55.05	.2294E+06	12.644	6.584		1.252	
											Triangle θ=30° Lift
2208030001	8.0	.311	.838	1.0	36.23	.1510E+06	5.697		6.849	1.303	
2208030002	8.0	.440	1.158	1.0	43.09	.1796E+06	7.872		6.689	1.272	
2208030003	8.0	.710	1.860	1.0	54.74	.2281E+06	12.644		6.658	1.266	
2208030004	8.0	.163	.431	1.0	26.23	.1093E+06	2.930		6.721	1.278	
2208030005	8.0	.238	.624	1.0	31.69	.1321E+06	4.242		6.664	1.267	

Table 14: Drag and Lift Coefficients - reduced data, 10° body b/B = 0.705

RUNNO	DIA	DELTAH	VOLT	GAIN	VELOCITY	REYNO	FORCE	CD	CL	CD1	SHAPE
1110000001	10.0	.100	.302	1.0	20.54	.1070E+06	3.063	9.161		.798	Circle Drag
1110000002	10.0	.145	.346	1.0	24.74	.1288E+06	3.509	7.239		.631	
1110000003	10.0	.190	.451	1.0	28.32	.1475E+06	4.574	7.201		.627	
1110000004	10.0	.265	.611	1.0	33.44	.1742E+06	6.197	6.994		.609	
1110000005	10.0	.407	.906	1.0	41.45	.2159E+06	9.189	6.753		.588	
2110000001	10.0	.102	1.748	1.0	20.75	.1081E+06	11.883	34.846		3.036	Triangle θ=0° Drag
2110000002	10.0	.140	2.350	1.0	24.31	.1266E+06	15.976	34.131		2.973	
2110000003	10.0	.190	3.223	1.0	28.32	.1475E+06	21.910	34.492		3.005	
2110000004	10.0	.260	4.377	1.0	33.13	.1725E+06	29.755	34.230		2.982	
2110000005	10.0	.300	5.085	1.0	35.58	.1853E+06	34.568	34.465		3.002	
2110030001	10.0	.100	.579	1.0	20.54	.1070E+06	3.936	11.773		1.026	Triangle θ=30° Drag
2110030002	10.0	.143	.834	1.0	24.57	.1280E+06	5.670	11.859		1.033	
2110030003	10.0	.191	1.120	1.0	28.39	.1479E+06	7.614	11.923		1.039	
2110030004	10.0	.269	1.543	1.0	33.69	.1755E+06	10.489	11.663		1.016	
2110030005	10.0	.418	2.423	1.0	42.00	.2188E+06	16.472	11.786		1.027	
2110060001	10.0	.103	.791	1.0	20.85	.1086E+06	5.377	15.615		1.360	Triangle θ=60° Drag
2110060002	10.0	.140	1.105	1.0	24.31	.1266E+06	7.512	16.049		1.398	
2110060003	10.0	.194	1.512	1.0	28.61	.1490E+06	10.279	15.847		1.381	
2110060004	10.0	.266	2.058	1.0	33.51	.1745E+06	13.990	15.731		1.370	
2110060005	10.0	.418	3.239	1.0	42.00	.2188E+06	22.019	15.756		1.373	
2210030001	10.0	.104	.659	1.0	20.95	.1091E+06	4.480		12.884	1.122	Triangle θ=30° Lift
2210030002	10.0	.145	.920	1.0	24.74	.1288E+06	6.254		12.901	1.124	
2210030003	10.0	.191	1.238	1.0	28.39	.1479E+06	8.416		13.179	1.148	
2210030004	10.0	.268	1.709	1.0	33.63	.1752E+06	11.618		12.966	1.130	
2210030005	10.0	.420	2.728	1.0	42.10	.2193E+06	18.545		13.207	1.151	

```
PROGRAM    STRLNO                    CDC 6600 FTN V3.0-P296 OPT=1   72/08/04. 20.06.31.

      C     PROGRAM STRLNO (INPUT,OUTPUT,TAPE 60=INPUT)
            TO FIND THE STROUHAL NUMBER,FLOW PROP.-68DEG F.
            INTEGER RUNNO,RUN1,RUN2
          5 FORMAT(1H1,/////6X,5HRUNNO,4X,4HSIZE,4X,6HDELTAH,6X,4HFREQ,
     5      12X,8HVELOCITY, 9X,5HREYNO,9X,1HS,8X,2HS1)
         10 FORMAT(I10,F5.1,F10.3,F10.2)
         20 FORMAT(1X,I10,F8.1,F10.3,2F10.2,E14.4,2F10.3)
         30 FORMAT(/)
            CTEMP=(460.+68.)/(460.+75.)
     10     RNU=0.000164
            GAMMA=0.07535*CTEMP
            DENSITY=0.00234*CTEMP
            B=14.1875
            CC=1.0
     15     PRINT 5
            SIZE2=1.0
            RUN2=0
         50 READ(60,10)RUNNO,SIZE,DELTAH,FREQ
            IF(EOF(60))110,60
     20     V=18.29*(SQRT(DELTAH/GAMMA))*0.975
            REYNO=(V*SIZE)/(12.*RNU)
            S=(FREQ*SIZE)/(12.*V)
            S1=S*(CC*(B-SIZE)/B)
            SIZE1=SIZE
     25     IF(SIZE1 .NE. SIZE2)GO TO 85
         83 RUN1=RUNNO/1000
            IF(RUN1 .NE. RUN2/1000)GO TO 90
            GO TO 95
         85 PRINT 5
     30     GO TO 83
         90 PRINT 30
         95 PRINT 20,RUNNO,SIZE,DELTAH,FREQ,V,REYNO,S,S1
            RUN2=RUNNO
            SIZE2=SIZE
     35     GO TO 50
        110 STOP
            END
```

Table 15 : Strouhal Number Program

Table 16: Strouhal number-reduced data, 1" body, b/B = 0.071

RUNNO	SIZE	DELTAH	FREQ	VELOCITY	REYNO	S	S1	SJ	Cc	SHAPE
1301000001	1.0	.147	62.50	25.07	.1274E+05	.208	.193			Circle 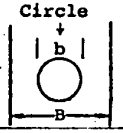
1301000002	1.0	.321	92.12	37.05	.1883E+05	.207	.193			
1301000003	1.0	.752	139.40	56.71	.2882E+05	.205	.190			
1301000004	1.0	1.395	186.00	77.24	.3925E+05	.201	.187			
2301000001	1.0	.135	42.77	24.03	.1221E+05	.148	.138	.110		Triangle θ=0° 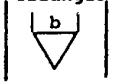
2301000002	1.0	.320	65.06	36.99	.1880E+05	.147	.136	.108		
2301000003	1.0	.760	101.79	57.01	.2897E+05	.149	.138	.110	.795	
2301000004	1.0	1.318	131.86	75.07	.3815E+05	.146	.136	.108		
2301000005	1.0	2.130	171.05	95.44	.4850E+05	.149	.139	.110		
2301030001	1.0	.143	54.84	24.73	.1257E+05	.185	.172			Triangle θ=30° 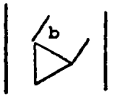
2301030002	1.0	.340	83.93	38.13	.1938E+05	.183	.170			
2301030003	1.0	.750	122.06	56.63	.2878E+05	.180	.167			
2301030004	1.0	1.350	160.00	75.98	.3861E+05	.175	.163			
2301030005	1.0	2.125	204.50	95.33	.4844E+05	.179	.166			
2301060001	1.0	.137	68.18	24.20	.1230E+05	.235	.218			Triangle θ=60° 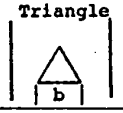
2301060002	1.0	.315	102.59	36.70	.1865E+05	.233	.217			
2301060003	1.0	.760	158.50	57.01	.2897E+05	.232	.215			
2301060004	1.0	1.293	206.00	74.36	.3778E+05	.231	.215			

Table 17: Strouhal number-reduced data, 2" body, b/B = 0.141

RUNNO	SIZE	DELTAH	FREQ	VELOCITY	REYNO	S	S1	SJ	Cc	SHAPE
1302000001	2.0	.133	32.10	23.85	.2424E+05	.224	.193			Circle
1302000002	2.0	.212	40.10	30.11	.3060E+05	.222	.191			
1302000003	2.0	.327	49.50	37.39	.3800E+05	.221	.190			
1302000004	2.0	1.057	87.50	67.23	.6832E+05	.217	.186			
2302000001	2.0	.323	36.70	37.17	.3777E+05	.165	.141	.106		Triangle θ=0°
2302000002	2.0	.540	48.06	48.05	.4884E+05	.167	.143	.107	.750	
2302000003	2.0	.725	55.80	55.68	.5659E+05	.167	.143	.108		
2302000004	2.0	1.024	65.90	66.17	.6725E+05	.166	.143	.107		
2302030001	2.0	.158	30.50	25.99	.2642E+05	.196	.168			Triangle θ=30°
2302030002	2.0	.234	36.80	31.63	.3215E+05	.194	.167			
2302030003	2.0	.330	43.30	37.57	.3818E+05	.192	.165			
2302030004	2.0	.526	54.69	47.43	.4820E+05	.192	.165			
2302030005	2.0	.715	65.50	55.30	.5619E+05	.197	.170			
2302060001	2.0	.155	36.87	25.75	.2616E+05	.239	.205			Triangle θ=60°
2302060002	2.0	.240	46.41	32.04	.3256E+05	.241	.207			
2302060003	2.0	.335	54.54	37.85	.3846E+05	.240	.206			
2302060004	2.0	.523	68.41	47.29	.4806E+05	.241	.207			
2302060005	2.0	.741	81.49	56.29	.5721E+05	.241	.207			
2302060006	2.0	1.012	94.89	65.78	.6685E+05	.240	.207			

Table 18: Strouhal number reduced data, 3" body, b/B = 0.212

RUNNO	SIZE	DELTAH	FREQ	VELOCITY	REYNO	S	S1	SJ	Cc	SHAPE
1303000001	3.0	.136	22.80	24.12	.3676E+05	.236	.186			Circle
1303000002	3.0	.225	29.20	31.02	.4729E+05	.235	.186			
1303000003	3.0	.330	35.10	37.57	.5727E+05	.234	.184			
1303000004	3.0	.454	41.50	44.06	.6717E+05	.235	.186			
1303000005	3.0	.621	48.40	51.53	.7856E+05	.235	.185			
2303000001	3.0	.230	23.15	31.36	.4781E+05	.185	.146	.105		Triangle θ=0°
2303000002	3.0	.335	28.08	37.85	.5770E+05	.185	.146	.105		
2303000003	3.0	.455	32.57	44.11	.6724E+05	.185	.146	.105	.720	
2303000004	3.0	.605	37.69	50.86	.7754E+05	.185	.146	.105		
2303000005	3.0	.840	44.64	59.93	.9136E+05	.186	.147	.106		
2303030001	3.0	.237	25.80	31.84	.4853E+05	.203	.160			Triangle θ=30°
2303030002	3.0	.330	30.40	37.57	.5727E+05	.202	.160			
2303030003	3.0	.465	36.60	44.59	.6798E+05	.205	.162			
2303030004	3.0	.624	42.00	51.66	.7875E+05	.203	.160			
2303030005	3.0	1.100	57.50	68.59	.1046E+06	.210	.165			
2303060001	3.0	.230	32.50	31.36	.4781E+05	.259	.204			Triangle θ=60°
2303060002	3.0	.324	38.25	37.22	.5674E+05	.257	.203			
2303060003	3.0	.455	45.40	44.11	.6724E+05	.257	.203			
2303060004	3.0	.650	55.20	52.72	.8037E+05	.262	.206			

Table 19: Strouhal number reduced data, 4" body, b/B = 0.282

RUNNO	SIZE	DELTAH	FREQ	VELOCITY	REYNO	S	S1	SJ	Cc	SHAPE
1304000001	4.0	.118	17.00	22.46	.4566E+05	.252	.181			Circle
1304000002	4.0	.200	22.50	29.24	.5944E+05	.256	.184			
1304000003	4.0	.265	25.60	33.66	.6842E+05	.253	.182			
1304000004	4.0	.313	28.00	36.59	.7436E+05	.255	.183			
1304000005	4.0	.665	41.50	53.33	.1084E+06	.259	.186			
2304000001	4.0	.183	18.80	27.97	.5686E+05	.224	.161	.113		Triangle θ=0°
2304000002	4.0	.260	22.20	33.34	.6777E+05	.222	.159	.112	.700	
2304000003	4.0	.655	35.40	52.92	.1076E+06	.223	.160	.112		
2304000004	4.0	1.215	48.30	72.08	.1465E+06	.223	.160	.112		
2304030001	4.0	.190	19.60	28.50	.5794E+05	.229	.165			Triangle θ=30°
2304030002	4.0	.275	23.40	34.29	.6970E+05	.227	.163			
2304030003	4.0	.322	25.30	37.11	.7542E+05	.227	.163			
2304030004	4.0	.662	37.10	53.21	.1081E+06	.232	.167			
2304030005	4.0	.900	43.10	62.04	.1261E+06	.232	.166			
2304060001	4.0	.192	24.40	28.65	.5824E+05	.284	.204			Triangle θ=60°
2304060002	4.0	.265	28.70	33.66	.6842E+05	.284	.204			
2304060003	4.0	.326	31.70	37.34	.7589E+05	.283	.203			
2304060004	4.0	.668	46.60	53.45	.1086E+06	.291	.209			

Table 20: Strouhal number reduced data, 6" body, b/B = 0.423

RUNNO	SIZE	DELTAH	FREQ	VELOCITY	REYNO	S	S1	SJ	Cc	SHAPE
1306000001	6.0	.116	14.21	22.27	.6790E+05	.319	.184			Circle
1306000002	6.0	.310	23.61	36.41	.1110E+06	.324	.187			
1306000003	6.0	.400	28.49	41.36	.1261E+06	.344	.199			
1306000004	6.0	.551	32.38	48.54	.1480E+06	.334	.192			
1306000005	6.0	.780	37.36	57.75	.1761E+06	.323	.187			
2306000001	6.0	.160	19.32	26.16	.7975E+05	.369	.213	.142		Triangle θ=0°
2306000002	6.0	.295	26.42	35.52	.1083E+06	.372	.215	.143		
2306000003	6.0	.405	31.11	41.62	.1269E+06	.374	.216	.143	.665	
2306000004	6.0	.530	35.12	47.61	.1451E+06	.369	.213	.142		
2306000005	6.0	.780	42.95	57.75	.1761E+06	.372	.215	.142		
2306030001	6.0	.158	16.08	25.99	.7925E+05	.309	.178			Triangle θ=30°
2306030002	6.0	.291	21.85	35.28	.1075E+06	.310	.179			
2306030003	6.0	.392	25.39	40.94	.1248E+06	.310	.179			
2306030004	6.0	.533	29.56	47.74	.1456E+06	.310	.179			
2306030005	6.0	.789	36.35	58.09	.1771E+06	.313	.181			
2306060001	6.0	.156	18.14	25.83	.7875E+05	.351	.203			Triangle θ=60°
2306060002	6.0	.291	25.26	35.28	.1075E+06	.358	.207			
2306060003	6.0	.392	29.30	40.94	.1248E+06	.358	.206			
2306060004	6.0	.539	34.07	48.01	.1464E+06	.355	.205			
2306060005	6.0	.785	41.31	57.94	.1766E+06	.356	.206			

```
PROGRAM  VORTEX                    CDC 6600 FTN V3.0-P296 OPT=1  72/08/17. 21.02.43.    PAGE    1

      PROGRAM VORTEX (INPUT,OUTPUT,TAPE 60=INPUT)
C     THE PURPOSE OF THIS PROGRAM IS TO FIND THE VORTEX STREET
C     PARAMETERS.
    5 FORMAT(1H1,/////1X,8HIDENTITY,3X,5HSTRNO,6X,2HCD,4X,3HH/L,4X,3HD/L
     1,1X,6HTRYD/L,3X,7H(D/L)CD,2X,3HL/D,3X,7HPERCENT)
   10 FORMAT(I7,F8.4,F8.2)
   15 FORMAT(1X,I8,F8.4,F8.2,3F7.4,F10.5,F5.2,F10.6)
   16 FORMAT(/)
   20 FORMAT(1X,I8,F8.4,F8.2,5X,15H**NO SOLUTION**)
      PRINT 5
      N=2200
   60 READ(60,10)IDENT,S,CD
      IF(EOF(60))110,70
   70 X=0.25
      DO 80 I=1,N
      FUNX=-7.1663*X**3+3.0271*X**2+1.8417*X-0.3792
      YCD=FUNX
      Y=FUNX/CD
      RY=1./Y
      SY=1.-S/Y
      C=EXP(3.1415926*X)
      CM=EXP(-3.1415926*X)
      COTH=(C+CM)/(C-CM)
      YN=X*(4.*SY*COTH-4.*X*COTH**2*SY**2)/CD
      IF(X .GT. 0.466)GO TO 100
      YP=(Y-YN)/Y
      IF(ABS(YP) .LT. 0.02 .OR. ABS(YP) .EQ. 0.02)GO TO 90
      X=X+0.0001
   80 CONTINUE
   90 PRINT 16
      PRINT 15,IDENT,S,CD,X,Y,YN,YCD,RY,YP
      GO TO 60
  100 PRINT 16
      PRINT 20,IDENT,S,CD
      GO TO 60
  110 STOP
      END
```

Table 21: Vortex Street Characteristics Program

IDENTITY	STRNO	CD	H/L	D/L	TRYD/L	(D/L)CD	L/D	PERCENT
1401000	.2034	1.22	.3343	.2517	.2468	.30704	3.97	.019227
1402000	.2195	1.46	.4618	.2816	.2760	.41109	3.55	.019939
1403000	.2351	1.52	**NO SOLUTION**					
1404000	.2543	1.89	**NO SOLUTION**					
2401000	.1479	2.38	**NO SOLUTION**					
2402000	.1652	2.83	**NO SOLUTION**					
2403000	.1852	3.63	**NO SOLUTION**					
2404000	.2232	4.34	**NO SOLUTION**					
2401030	.1808	1.99	**NO SOLUTION**					
2402030	.1939	2.14	**NO SOLUTION**					
2403030	.2046	2.42	**NO SOLUTION**					
2404030	.2299	2.61	**NO SOLUTION**					
2401060	.2291	1.44	**NO SOLUTION**					
2402060	.2440	1.59	**NO SOLUTION**					
2403060	.2570	1.98	**NO SOLUTION**					
2404060	.2874	2.29	**NO SOLUTION**					

Table 22: Output - Vortex Street Program